Agenzia nazionale per le nuove tecnologie,
l'energia e lo sviluppo economico sostenibile

MINISTERO DELLO SVILUPPO ECONOMICO

Ricerca di Sistema elettrico

Rapporto sulla progettazione finale del Target Assembly a baionetta completo di disegni e dei dispositivi per la sua manutenzione remotizzata

D. Bernardi, M. Porfiri, T. Pinna, M. Frisoni, G. Micciché, M. Serra

con il contributo di:
P.A. Di Maio, P. Arena, G. Bongiovì
B. Knaepen, A. Prakash, M. Caby
F. Becchi, M. Morando

Report RdS/2013/130

RAPPORTO SULLA PROGETTAZIONE FINALE DEL TARGET ASSEMBLY A BAIONETTA COMPLETO DI DISEGNI E DEI DISPOSITIVI PER LA SUA MANUTENZIONE REMOTIZZATA

D. Bernardi, M. Porfiri, T. Pinna, M. Frisoni, G. Miccichè, M. Serra (ENEA)

Con il contributo di:

P.A. Di Maio, P. Arena, G. Bongiovì (Università di Palermo)
B. Knaepen, A. Prakash, M. Caby (Università di Bruxelles, ULB)
F. Becchi, M. Morando (Telerobot SpA)

Settembre 2013

Report Ricerca di Sistema Elettrico

Accordo di Programma Ministero dello Sviluppo Economico - ENEA
Piano Annuale di Realizzazione 2012
Area: Produzione di energia elettrica e protezione dell'ambiente
Progetto: Attività di fisica della fusione complementari a ITER
Obiettivo: Progettazione e qualifica ingegneristica del target IFMIF
Responsabile del Progetto: Ing. Aldo Pizzuto, ENEA

Index

Summary

The International Fusion Materials Irradiation Facility (IFMIF) is an international joint project aimed at developing an accelerator-based neutron irradiation facility to test and qualify candidate materials to be used in future fusion power reactors. Within the current IFMIF Engineering Validation and Engineering Design Activities (EVEDA) phase, ENEA is involved, as officially stated in the Procurement Arrangement ED03-EU, in the design of the Target Assembly (TA) with removable bayonet Backplate which is one of the two alternative concepts envisaged for the TA system of IFMIF (the other being the Integral Target Assembly to be developed by JAEA in Japan).

In the present annual period (PAR 2012) covered by the current MSE-ENEA Agreement, the design of the Target Assembly with bayonet Backplate has advanced starting from a previous reference model based on the design described in the Design Description Document-II (DDD-II) related to the second phase of the European Engineering Design Activities (EDA), as well as in the last MSE-ENEA Agreement report (PAR 2011). The current status of the TA design has been reported in the final Design Description Document- III (DDD-III) at the end of the third and last phase of the IFMIF/EVEDA EDA.

The work has consisted, in particular, in the advance of the TA model up to the present final state and in a detailed supporting analyses including nuclear, thermomechanical and thermohydraulic simulations through qualified numerical codes.

In the present document, a detailed description of all the above mentioned activities is reported.

1 Introduction

In the framework of the European Engineering Design Activities (EDAs) of IFMIF/EVEDA project, ENEA is committed to providing the engineering design of the Target Assembly with bayonet Backplate. The whole workpackage is defined in the IFMIF Procurement Arrangement ED03-EU [1] which is integrated by the complementary JAEA Procurement Arrangement (ED03-JA) [2] to establish the overall work for the design of the entire IFMIF Lithium Target Facility.

2 Engineering Design of EU IFMIF Target Assembly system

In the following, a brief description of the technical work performed and of the results obtained in the present annual period covered by the current MSE-ENEA Agreement is reported.
The performed work includes, in particular:

a) the update and progress of the TA design up to the present final state, starting from the available configuration developed within the previous annual period of the MSE-ENEA Agreement [3]

b) the detailed numerical analyses carried out in support to the above design activities. In particular, nuclear, thermomechanical and thermohydraulic analyses have been performed.

2.1 Finalization of the TA design

The Target Assembly design has been progressed to a well-advanced stage, although some work still remains to be done to fully complete some features and achieve an optimized configuration. The current status of the TA design has been reported in the final Design Description Document- III (DDD-III) [4] at the end of the third and last phase of the IFMIF/EVEDA EDA. The most updated 3D model of the system is shown in Fig. 2.1. The corresponding 2D sketch with main dimensions is given in Fig. 2.2.

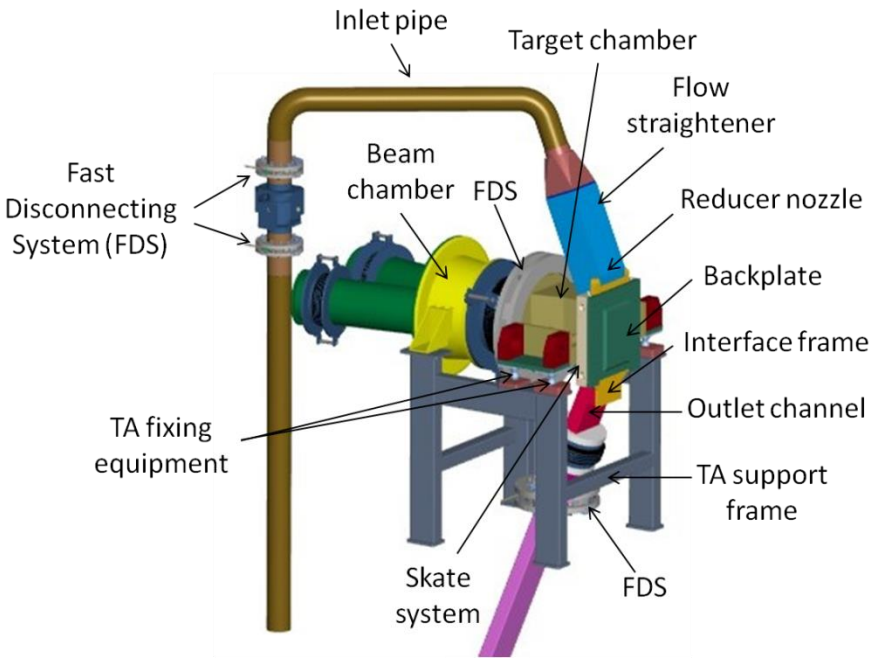

Fig. 2.1 - Final 3D model of the TA system

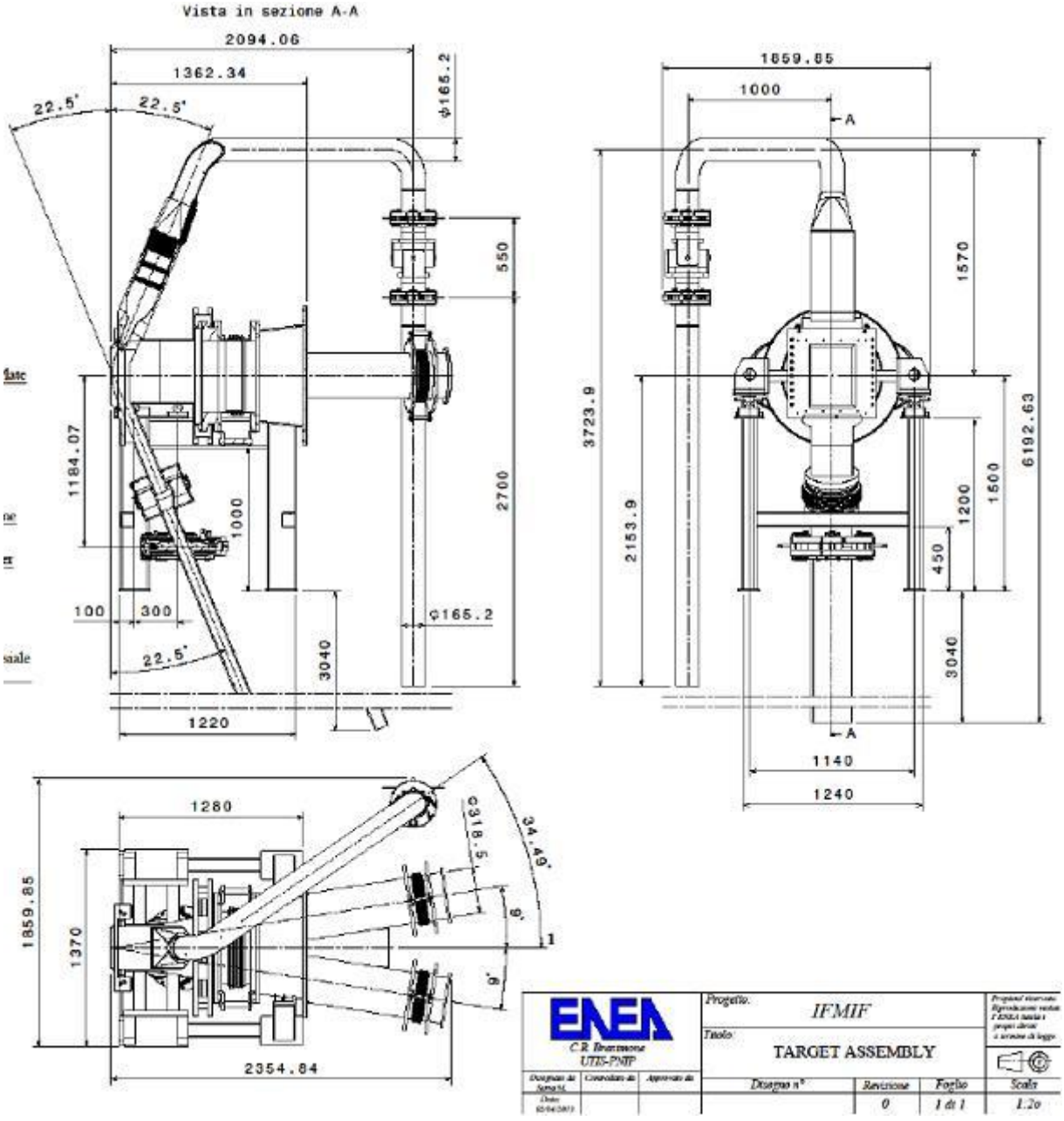

Fig. 2.2 - 2D sketch of the TA system

Compared to the previous version, the following modification and integrations have been introduced:

- The lithium leak detector system has been added on the backplate
- The compensating bellows system has been revised
- The outlet channel configuration has been changed to take into account JAEA modifications and simplify the remote-handling operations (in particular, the connecting flange with the fixed part of the outlet duct has been placed in horizontal position to facilitate the alignment of the TA during its insertion)
- The updated design of the three Fast Disconnecting Systems (FDS) for the connection of the TA with the lithium loop and the accelerator beam duct have been integrated in the model
- The design of the main RH tools specific for the TA and the BP has been realized (by Telerobot SpA) and the related RH procedures have been defined through software simulation

A description of the main TA subsystems affected by these modification is briefly reported hereafter.

Removable backplate

The removable backplate is a nearly square plate (Fig. 2.3) suitably designed to create, once it is clamped on the fixed frame, the concave channel for the lithium flow, assuring at the beam footprint region the specified thickness (1.8 mm) to guarantee the required neutron flux to the test modules. Overall dimensions are 630 mm x 604 mm. The current bayonet concept foresees the extraction/introduction of the BP from the top of the fixed frame, by sliding it along the vertical direction.
A suitable rectangular gasket is placed between the BP and the frame to properly assure the sealing between the two components. The required seating load on the gasket (180 N/mm) is produced by the combined action of eight M10 bolts (four in the upper part and four in the lower part) and two skate systems (at the BP lateral sides). Since the inevitable lithium penetration between the BP and the frame might hinder the detachment of the two components during the BP removal, four detachment screws are also introduced to assure the required detachment force. All tightening bolts and detachment screws are coated with an anti-seizure material (e.g., dicronite or silver) to avoid their blockage potentially caused by the severe operating conditions to which they are subjected inside the Test Cell. Qualification of silver-coated and dicronite-coated bolts is underway. Preliminary tests performed at ENEA Brasimone seem to indicate that silver coatings behave better than dicronite at least for what concerns the only effect of temperature. Further tests are however needed to confirm this conclusion. Moreover, the effect of nuclear swelling which poses constraints on the maximum allowable irradiation dose (and thus on the BP lifetime) has also to be taken into account. The effect of nuclear swelling on the tightening bolts has been numerically studied in a recent past [5] but needs to be revised in light of the updated neutronic results now available. Each skate system is rigidly connected to the BP through a series of M10 bolts. This solution allows the whole skate system to be completely replaced together with the BP, since the two elements forms a single removable component.

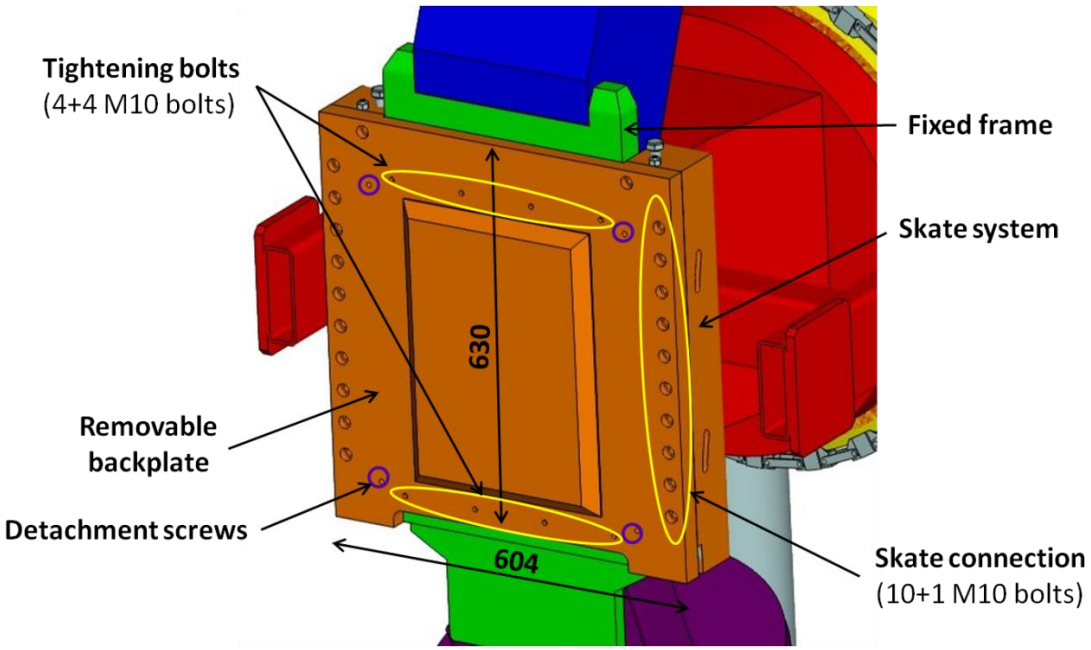

Fig. 2.3 – Rear view of the backplate

A rectangular groove is machined on the front side of the BP to house the gasket (Fig. 2.4). Four staggered spacers (two in the upper part which are staggered with respect to the other two in the bottom part) are introduced to prevent the impact of the BP against the frame during its insertion/extraction and the possible consequent damage of the gasket. Of these four pin spacers, the upper ones are placed on the frame (being the corresponding holes on the BP), while the lower ones are fixed to the BP (being the corresponding holes on the frame).

A leak detection system based on the concept of an electric contact probe is foreseen to fulfill safety requirement by detecting potential lithium spills at the BP/frame interface. The Li detector device is the same adopted for the FDS flanges and is simply composed by two metal wires inserted in a series of ceramic spacers to form a rectangular collar (Fig. 2.5) which is placed in a dedicated groove running all along the outside perimeter of the gasket (Fig. 2.4).

The Li flow channel is shaped on the BP front according to the profile geometry with variable curvature developed by ENEA. Unlike the ELTL TA, in the IFMIF TA design the Li profile is entirely housed on the BP (no straight parts are foreseen) in order to have only one interface (nozzle/BP interface, see Fig. 2.6) instead of two (nozzle/frame and frame/BP interfaces) so reducing potential misalignments issues of the channel parts which might cause fluid-dynamic instabilities. Lithium exiting from the reducer nozzle injects directly into the curved channel on the BP where the centrifugal force increases its local pressure in order to prevent boiling.

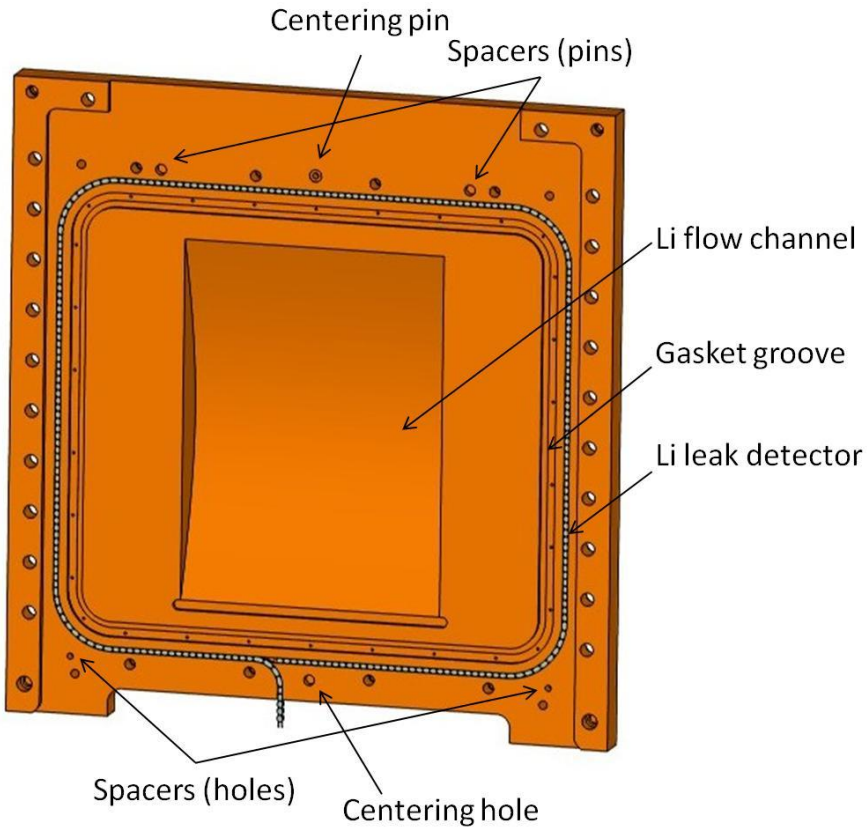

Fig. 2.4 – Front view of the backplate

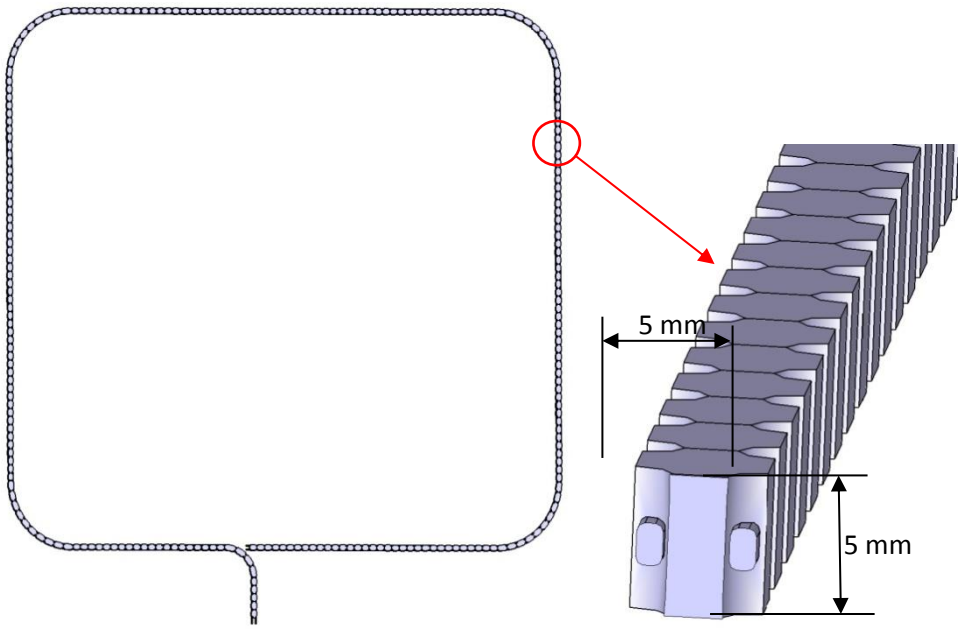

Fig. 2.5 – Detail of BP Li leak detector

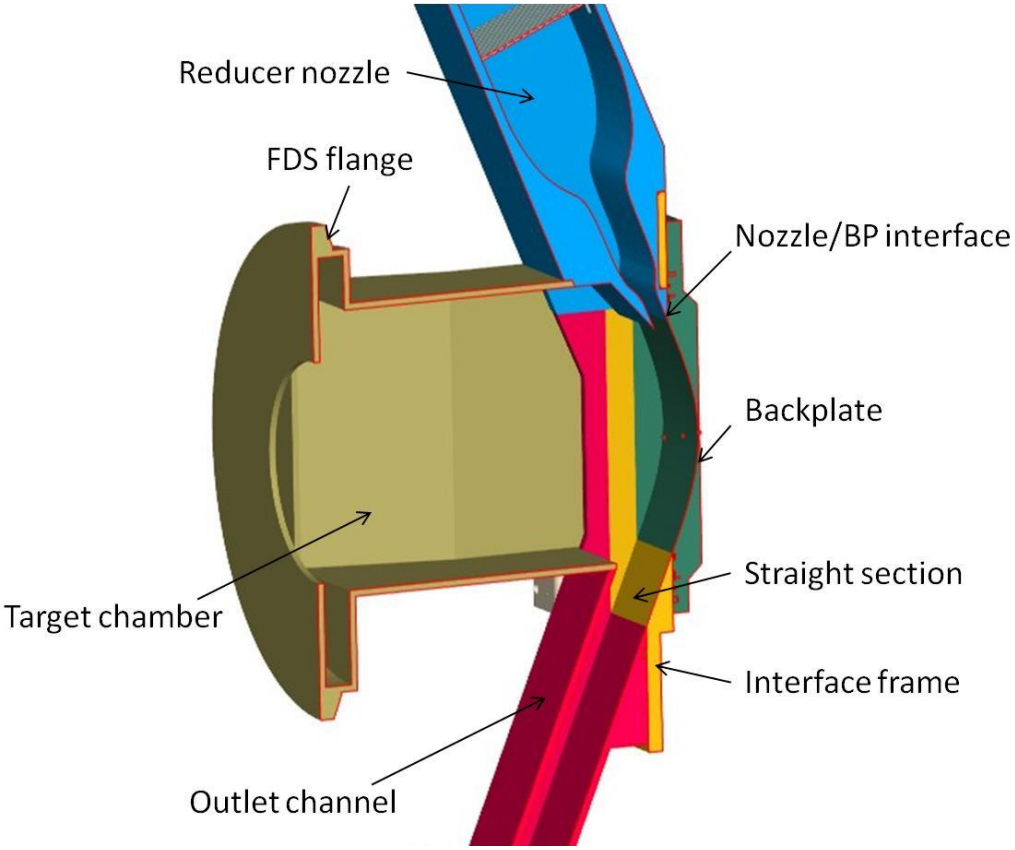

Fig. 2.6 – Flow channel with nozzle/BP interface

Inlet pipe and bellows compensating system

A short stretch of lithium pipe belongs to the TA system and is therefore removed along with the TA itself. This pipe has the function to physically connect the TA system to the fixed part of the main Li loop, routing the Li into the flow straightener before it is injected in the reducer nozzle. The TA inlet pipe is connected through a mechanical flange to the upper end of the fixed inlet pipe penetrating the Test Cell floor. A Fast Disconnecting System (FDS) is foreseen for this connection to simplify TA replacement operations and reduce the maintenance intervention times. Following JAEA dimensioning of the integral TA inlet pipe [6], a 6B tube with Sch. 40 is assumed. Since the material of the main TA section is EUROFER while that of the pipe, expansion joint and FDS flanges is SS316L, heterogeneous welds are envisaged. Feasibility of dissimilar welds has been successfully demonstrated, although their capability to withstand radiation exposure is still to be fully assessed [6].

A cardan (gimbal) expansion joint able to compensate angular movements in every plane is introduced on the vertical section of the inlet pipe (Fig. 2.7) to compensate thermal expansions during operation and manufacturing misalignments during installation. A detailed sketch of the cardan expansion joint is shown in Fig. 2.8. This type of joint has the advantage of being self-balanced, i.e. there is no need of fixed points on the pipe. Moreover, it can be equipped with an inner sleeve to smooth the flow and limit the direct exposure of the bellow with the flowing lithium so reducing the erosion effect. In any case, an additional FDS is foreseen to easily allow for the replacement of the joint in case that its lifetime is shorter than that of the TA.

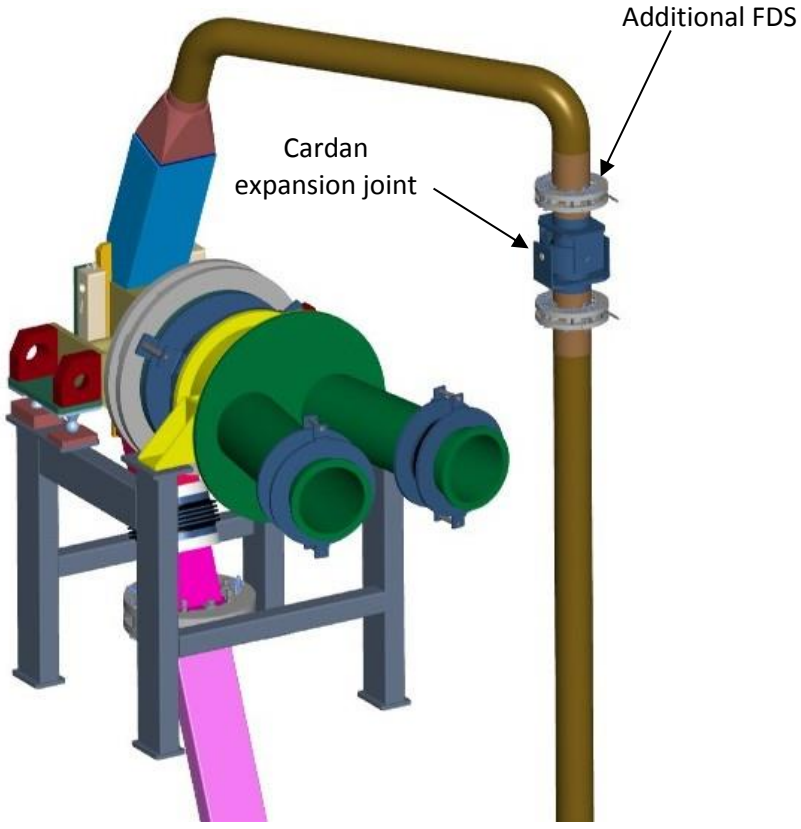

Fig. 2.7 - Inlet pipe compensation

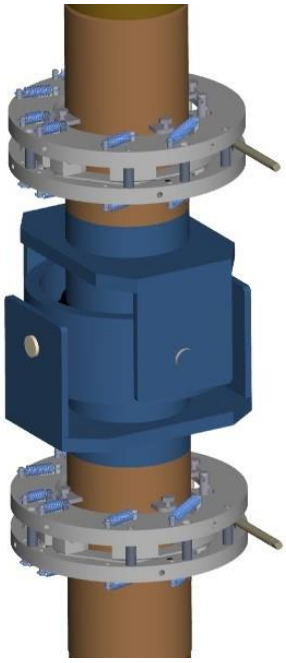

Fig. 2.8 - Detail of the cardan expansion joint

Outlet channel

The outlet section consists mainly of a rectangular channel (Figs. 2.9 and 2.10) that connects the BP to the upper end of the outlet pipe penetrating the test Cell floor and which injects, at the opposite end, into the Quench Tank. A FDS is foreseen for the channel/pipe connection. An axial expansion joint is placed close to the connection with the functions of absorbing the thermal dilatations of the channel and compensate little misalignments during installation. Unlike the DDD-II design, the FDS flanges are now placed horizontally to facilitate the RH operations during the installation of the TA.

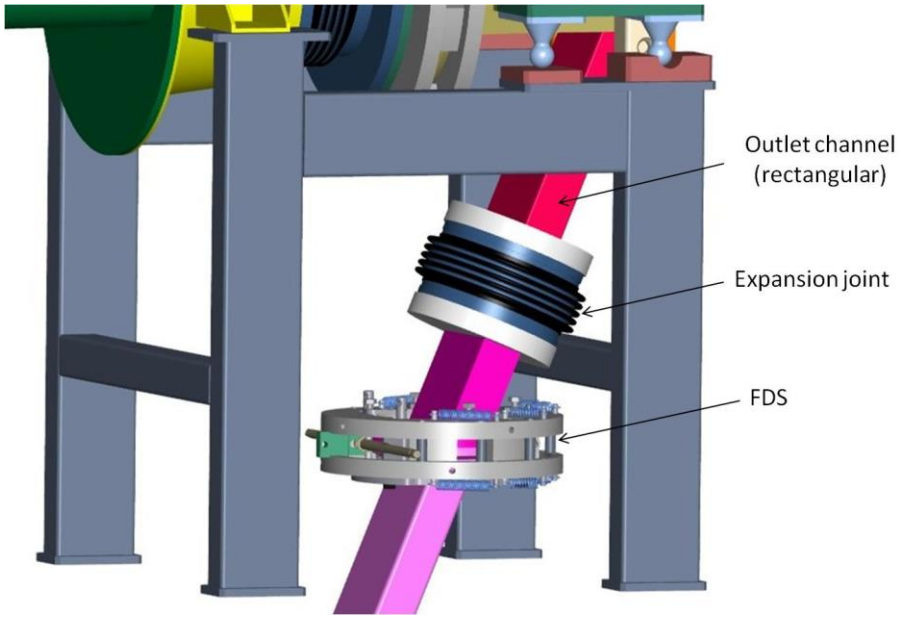

Fig. 2.9 – Outlet channel

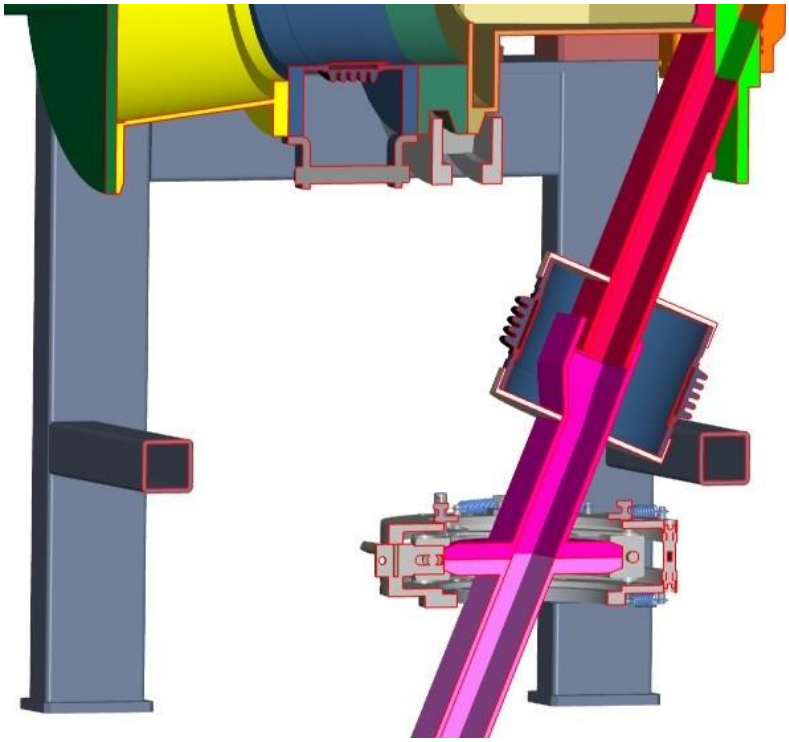

Fig. 2.10 – Section view of the outlet channel

FDS connections

A Fast Disconnecting System (FDS) is used as flanged connection of the TA inlet and outlet pipes with the lithium loop and of the target chamber with the accelerator beam duct. This system permits to easily and quickly connect and disconnect the flanges by simply acting (by remote) on only one screw. The design of the FDS for the inlet connection has been completed according to the specification given in Tab. 2.1.
A 3D view of the system is shown in Fig. 2-11.
It consists of a collar chain that provides, through a number of clamping sections, the force needed for compressing the sealing gasket between the flanges; opening and closing of the chain mechanism is obtained by maneuvering only one screw. Apart from the removable flange and the gasket which are removed together with the TA, the rest of the FDS is attached to the fixed part of the pipe so that it remains in position in the Test Cell when the TA is removed. The design of the system also comprises the following features:

- a supporting plate for the system replacement
- a Li leak detection system;
- an emergency unlocking system allowing the FDS opening in case of failure
- a removable insulation system

A 2D sketch of the FDS showing its main dimensions with and without insulation system is illustrated in Figs. 2.12 and 2.13, respectively.
The FDS for the outlet and beam connections are still under development, therefore they have been introduced in the CAD file by simply scaling the FDS design for the inlet connection.

Tab. 2.1 - Design specifications for the FDS inlet connection

Item	Requirement
Operating temperature	250° C
Design temperature	350° C
Environment	Lithium in contact
Internal operating pressure	0.2 MPa
External operating pressure	5 kPa - 0.1 MPa
Design inner Δp (p_{in}- p_{out})	0.43 MPa
Design outer Δp (p_{out}- p_{in})	0.1 MPa
Bolting points	1
Pipes dimension	6" Sch. 40
Type of gasket	Helicoflex metallic gasket
Max leak rate (He)	10^{-7} Pa m^3/s
Insulation Temperature	350° C → 50° C
Insulation material	PYROGEL XT (TBC)
Seizure prevention	Use of antifriction material (TBD)

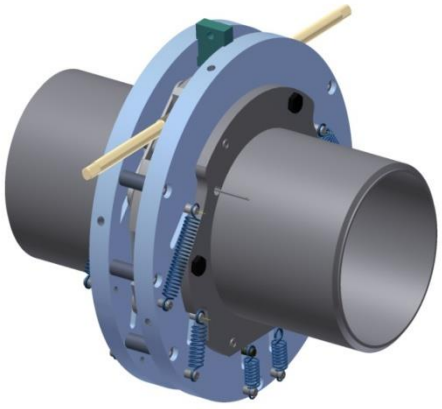

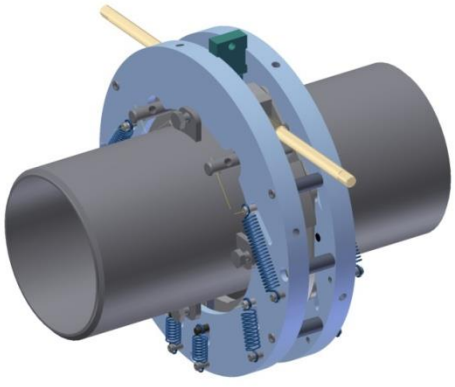

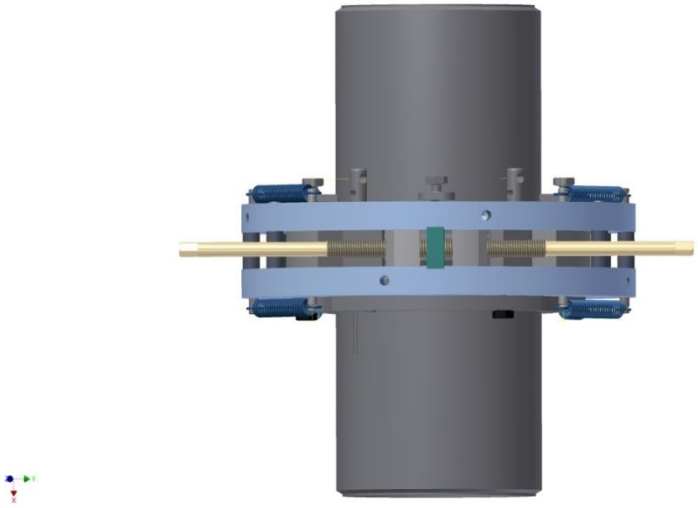

Fig. 2.11 – 3D views of the FDS for the inlet connection

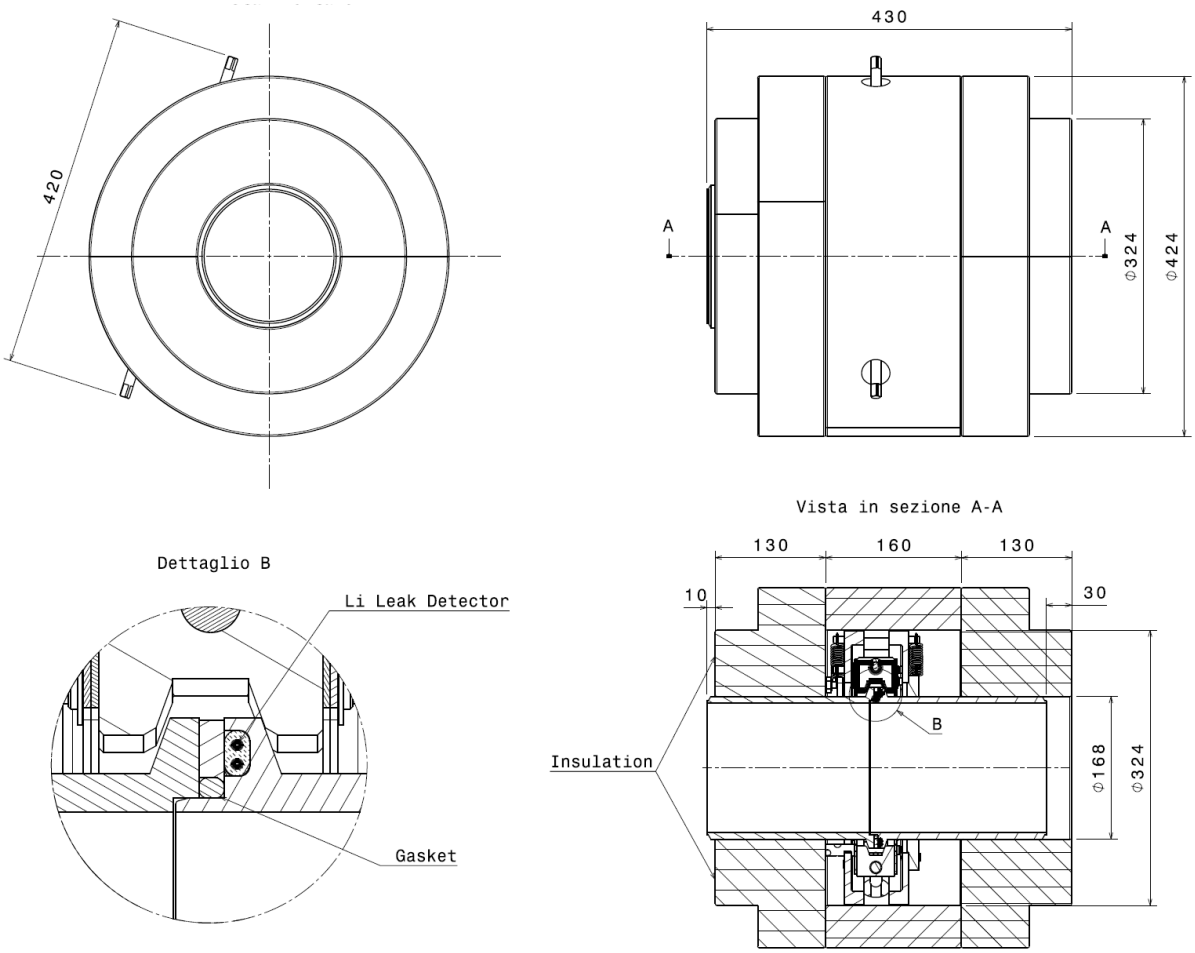

Fig. 2.12 – Sketch of the inlet FDS with insulation system

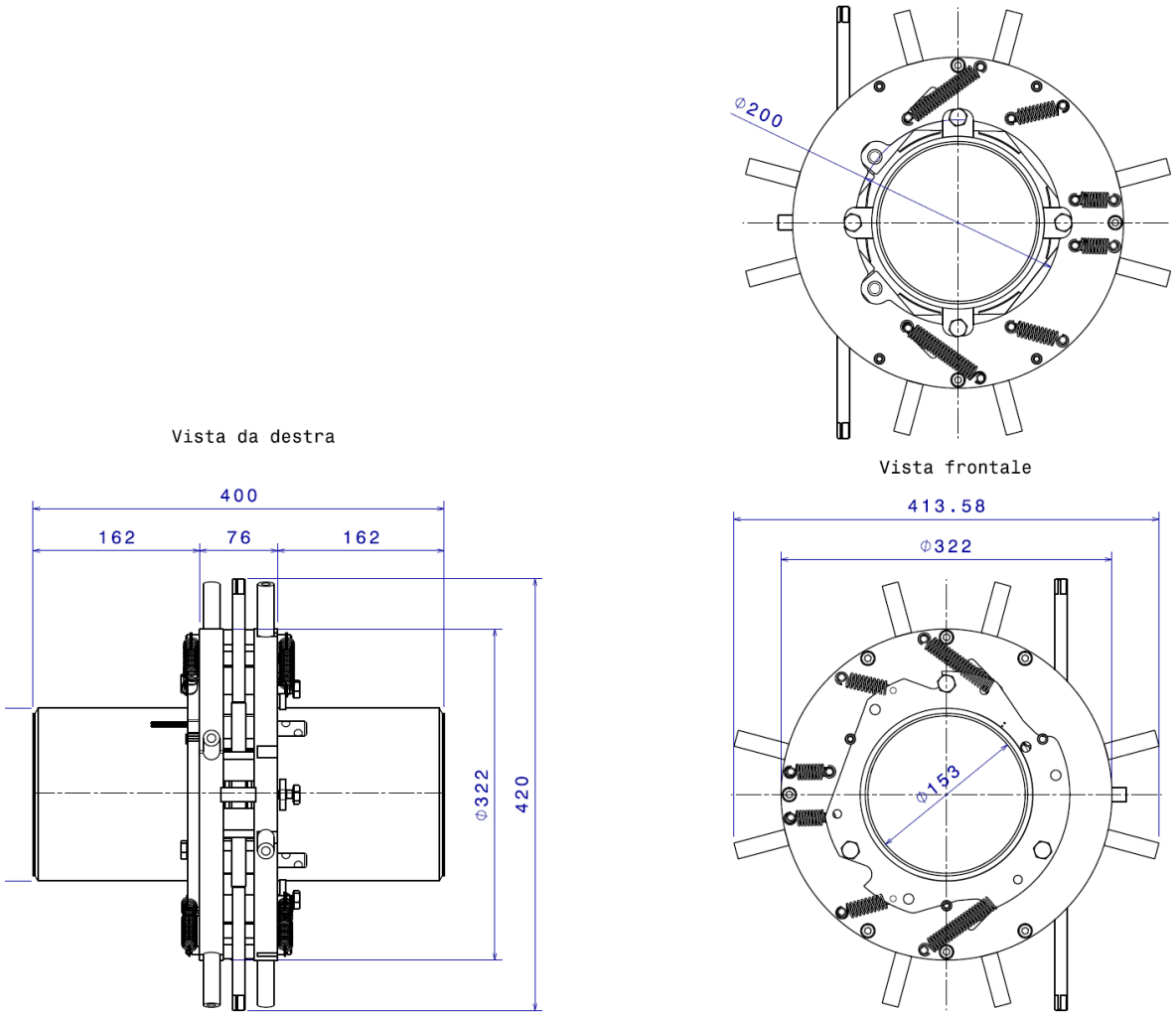

Fig. 2.13 - Sketch of the inlet FDS without insulation system

Design of the RH tools

Almost all the preventive maintenance of the IFMIF components will be performed during the annual shutdown of the facility. Duration of this maintenance period is 20 days, of which seven days will be devoted to perform the maintenance of the TA. However, due to the exposition of this component to the high neutron flux its substitution/refurbishment could be required even more frequently. Accordingly, two different scenarios are considered for the refurbishment of the TA:

- substitution of the entire TA
- substitution of the BP only

The first option is adopted for the annual preventive maintenance while the latter is devised in case of a reduced life time of the BP or of other components which entail intermediates maintenance activity. It should be noted that BP exchange during the annual preventive maintenance cannot be a priori excluded. The intervention times in both scenarios are comparable even if at present there are several uncertainties that can be only clarified later on after the completion of the validation activities: particular attention has to be paid to the erosion/corrosion in the nozzle and flow channel. Lifetime of other critical components

such as gaskets, diagnostics, ecc. should also be checked although it is not expected that these will strongly affect scheduled maintenance duration.

- *Robotic devices*

A set of custom made devices is moved inside the test cell using a crane that moves a vertical boom for in cell positioning. The following picture shows a sectional view of the Test Cell and of the hall above with the crane above the opened Test Cell with boom fully deployed.

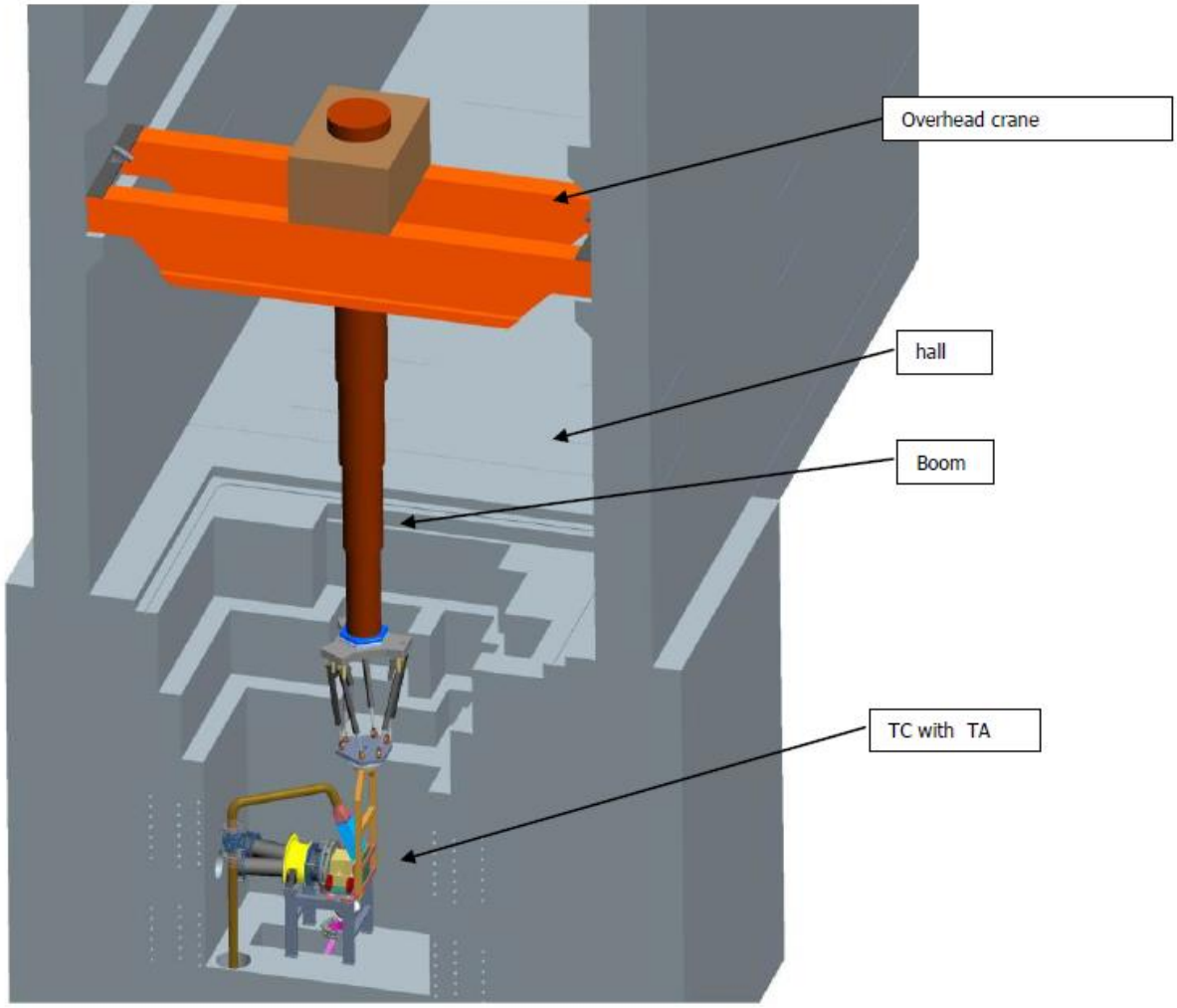

Fig. 2.14 - Overhead crane layout

At the end of the boom a parallel kinematic manipulator (PKM) or hexapod allows the precise tools displacement with respect to the TA. A 7 DOF (Degrees of Freedom) robotic arm is used alternatively for in cell manipulation.
The remote handling and maintenance strategy is based on the idea of a reconfigurable modular device connected to the Test Cell overhead crane.
A quick disconnect flange or Gripper Change System (GCS) is located at the crane boom end plate. The mating flange is connected to the different positioners, manipulators and tools.
The GCS first link mechanically the tool with the base device; a set of front mating connectors link then the used devices with the power supply and control cabinets once the flange is connected/locked.
The GCS solution is frequently used in industrial automation to change a robot tool (these devices are also called tool changers) but bigger GCS size (recently introduced in the industrial market for increased robot payload) can be took as first feasibility check for a GCS able to support a complete manipulator.

For bigger flexibility and to reduce at the same time the number and dimensions of positioner/manipulator both the PKM and the 7dof robot have a GCS on their base, to connect the manipulator/positioner to the crane, and a second smaller unit to connect the positioner/manipulator to its tool.
Each GCS is based on one/three docking plugs that link rigidly the two flanges (male and female). The dimension and number of the plugs is related to max forces/torques supported by the connection. Each plug is based on a pneumatic expansion plug that push several steel spheres in a expressly made receptacle. Conical plugs on calibrated holes complete the mechanical connection and ease the GCS alignment and coupling.
For safety reason (the GCS can generally lift relevant weight) the expansion plug used to close the GCS is generally bi-stable and switch from "closed" to "open" position only with an active command: the GCS with pressure cut/no power keep the tool/device connected in a “safe” configuration (the GCS hold the lower flange connected and locked but loose precision for pressure drop).
IFMIF BP/TA refurbishment devices will adopt three different GCS:

- Main GCS between overhead crane boom and PKM/7 DOF RBT manipulators rated preliminarily for 3300 kg;
- Secondary GCS between PKM and BP/TA gripper, rated for 1200 kg;
- Tool GCS between 7 DOF robot tool plate and tools, rated for 30 kg.

Preliminary verification made on commercial off-the-shelf flange shown that a limited intervention on material could be needed to have a "rad hard' rated flange (typically elastomers, plastic and grease).
Following picture shows the commercial version of a high load GCS (1350 kg nominal load) with no electrical connection shown (electrical modules can be connected on the GCS sides)

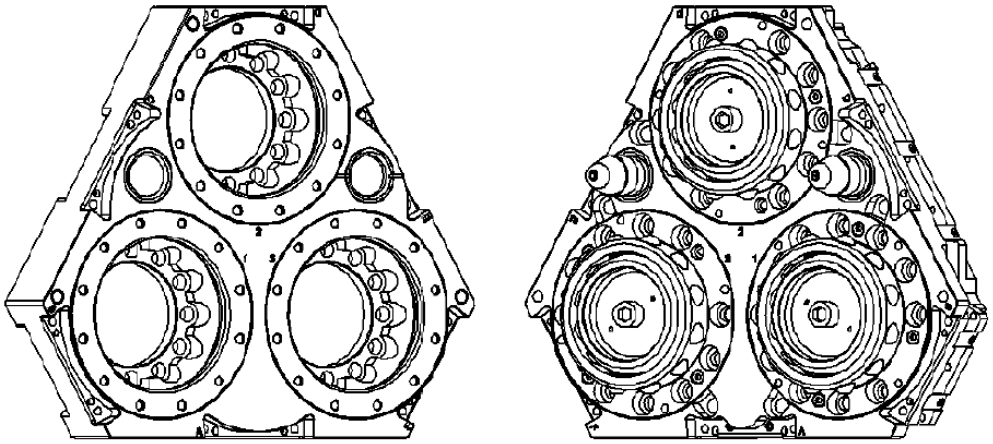

Fig. 2.15 - Gripper Change System (GCS)

Another relevant advantage of the GCS geometrical configuration is the misalignment tolerance in the GCS docking. The following picture and table, took from the same GCS shows maximum linear and angular alignment mismatch for the above shown commercial flange.

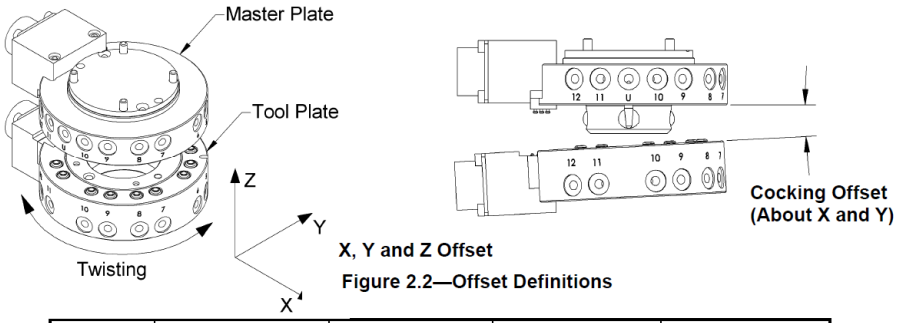

Figure 2.2—Offset Definitions

Model	No-Touch™ Zone Z Offset (Max)* (mm)	X and Y Offset (Max)† (mm)	Cocking Offset (Max) (degrees)	Twisting Offset (Max) (degrees)
QC-1210	1	±2	±0.7	±1

Fig. 2.16 - GCS alignments tolerance

The PKM used follows the standard Stewart 6 DOF platform configuration: the upper frame is rigidly connected (by means of a GCS) with the overhead crane boom while the lower flange is connected to the upper one with 6 linear actuators in parallel. Preliminarily each actuator has a nominal stroke of 1000 mm and a nominal thrust force of 20 KN (MOOG Max force actuator size 4 is kept as industrial equivalent reference). Preliminary motion ranges and performances are reported in the following table.

Tab. 2.2 - PKM reference data

Direction	Range	Speed
Vertical (Z)	+/- 500 mm	30 mm/s
Horizontal (X,Y)	+/- 500 mm	30 mm/s
Z axis rotation	+/- 120°	5°/s
X/Y rotation	+/- 45°	5°/s

The following pictures show main PKM components and overall dimensions (in closed configuration vertical end of stroke)

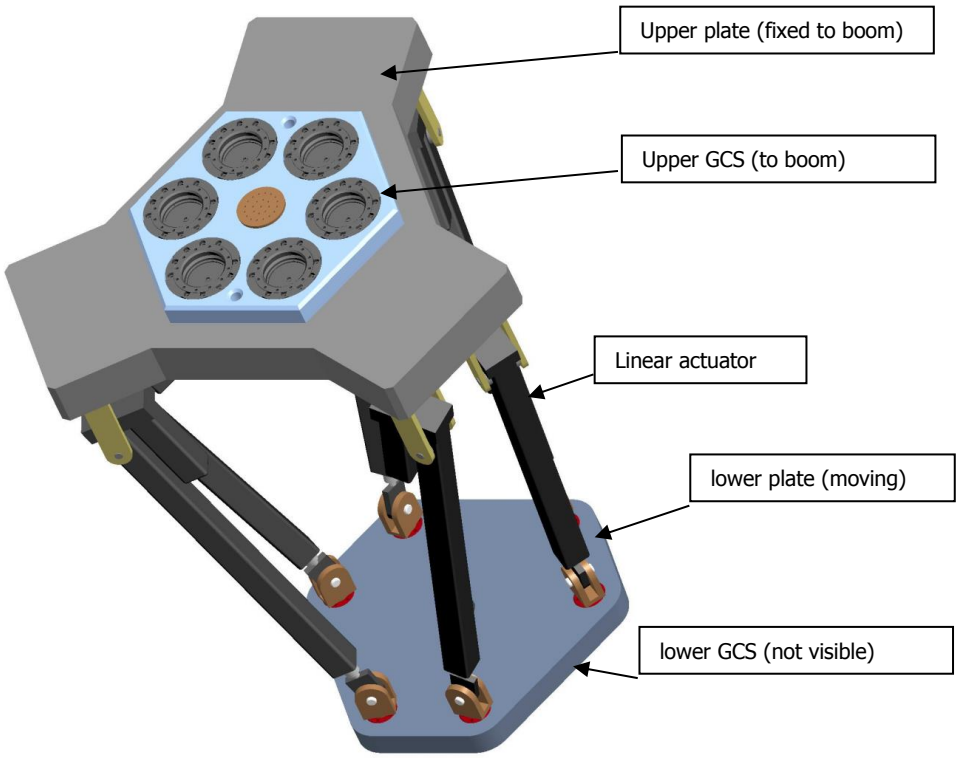

Fig. 2.17 - PKM general view

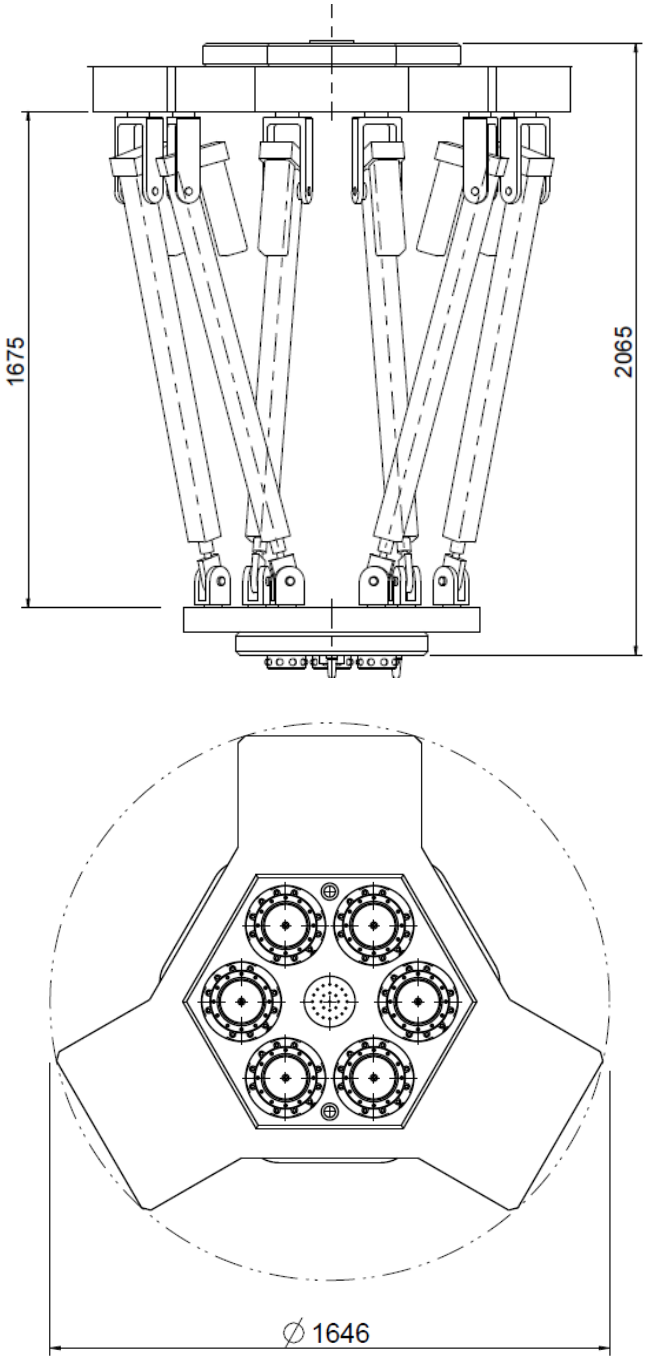

Fig. 2.18 - PKM dimensional view (front and top view)

Expected tasks that will be performed with the PKM are:

- Backplate removal/insertion (using a dedicated tool connected to the PKM moving plate);
- Full TA removal and positioning (using a dedicated support frame to support the TA).

The kinematic structure of the PKM allow precise positioning of TA and BP in the space without the need of a crane repositioning. The crane should approach the target position and the PKM should complete the task with no further crane motion.
The big advantage of a PKM robot is that motion and positioning involve only small masses and inertia of the PKM. The parallel layout of the manipulator ensures also high stiffness and limit the potential

conflicts/interferences with the test cell structures/modules: similar payload serial arm would require bigger actuator size (each joint starting from the shoulder support the full load and the following joints) resulting, in this particular case, in a unfavorable ratio btw robot weight/dimension and used/needed workspace (the cell boundaries limit the positioner workspace).
Each PKM link will be based on a recirculating ball screw connected to an high performance brushless motor, an absolute position sensor and a force (thrust) sensor.

The second device foreseen to perform support intervention in the IFMIF test cell is a seven degrees of freedom serial manipulator. It is used to bring the various RH tools in side of the TC .
Overall arm dimensions are shown in the pictures that follows. Nominal payload in this case is 30 kg.
The robot shoulder will be connected to a quick disconnect female flange trough a boom, preliminarily 2.6 m long, needed to correctly off-set the robot workspace with respect to the overhead crane boom and to reach outlet FDS for TA removal and flange cleaning.
The robot shown in the simulations dimensionally starts from the Yaskawa SA20 with the perspective of review the payload/speed ratio adopting some component modification to match Rad Hard requirements.

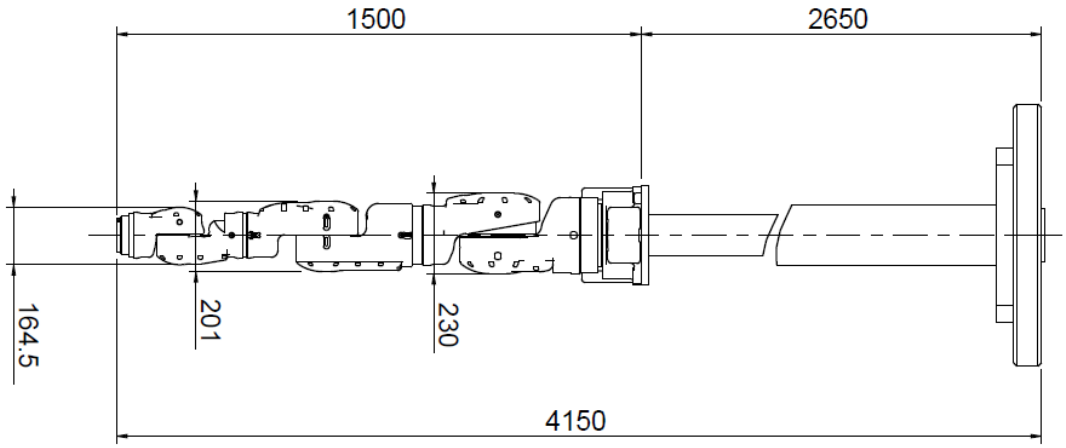

Fig. 2.19 - 7 DOF robotic arm general dimensions (with boom and GCS interface shown)

The redundant full anthropomorphic actuator disposition is mandatory to compensate the motion constraint in tight environment. The rotational degrees of freedom between shoulder and elbow pitch allow the elbow re-orientation needed to correctly access, as a relevant example, the lower FDS or the BP unlocking/extraction screws. The robotic arm will be provided with suitable gripper to interface all the RH tools.

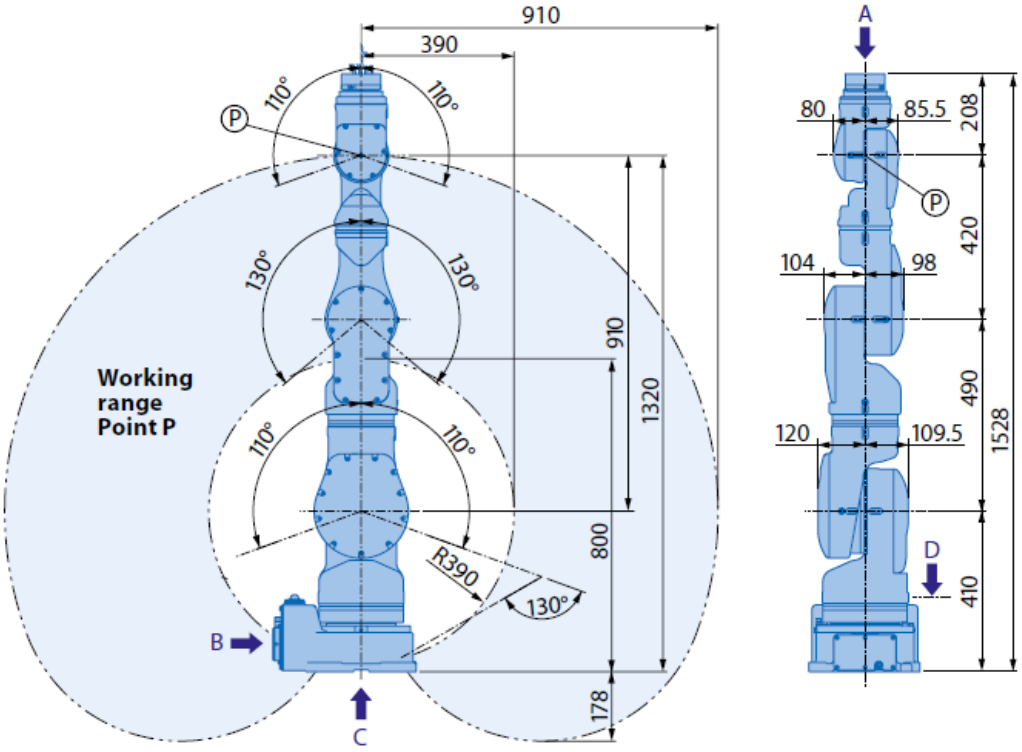

Fig. 2.20 - 7 DOF RBT dimensions

Preliminary arm motion ranges/performances from shoulder to wrist are below resumed.

Tab. 2.3 - 7 DOF robot reference data

Axis	Range (°)	Speed (°/s)
1	+/-180	65
2	+/-110	65
3	+/-170	85
4	+/-130	85
5	+/-180	100
6	+/-110	100
7	+/-180	200

Expected tasks that will be performed with the 7 DOF robot are:

- FDS opening;
- Beam bellow opening;
- BP unbolting;
- Cleaning.

- *BP gripper*

The BP gripper is based on a machined welded frame that can be connected to the PKM tool plate. The gripper frame allows correct BP alignment/positioning on the TA with no interferences with modules (HFTM being removed) and with the target. The BP is connected to the BP gripper with 4 actuated pins that are inserted in 4 “ad-hoc” holes made in the two BP side guides. Connection pin can be actuated in three different position:

- With pins “out”: BP is free from the gripper;
- With pins “full-in”: BP is rigidly connected to the gripper;
- With pins “half-in”: there is some play between gripper and BP that allow BP extraction leaving some residual freedom of displacement to the BP with respect to the gripper.

While the second configuration is needed to precisely position the BP on the TA at the end of maintenance/refurbishment the third configuration can be used to remove the BP from TA with looser precision in case of, for example, damaged or deformed BP.

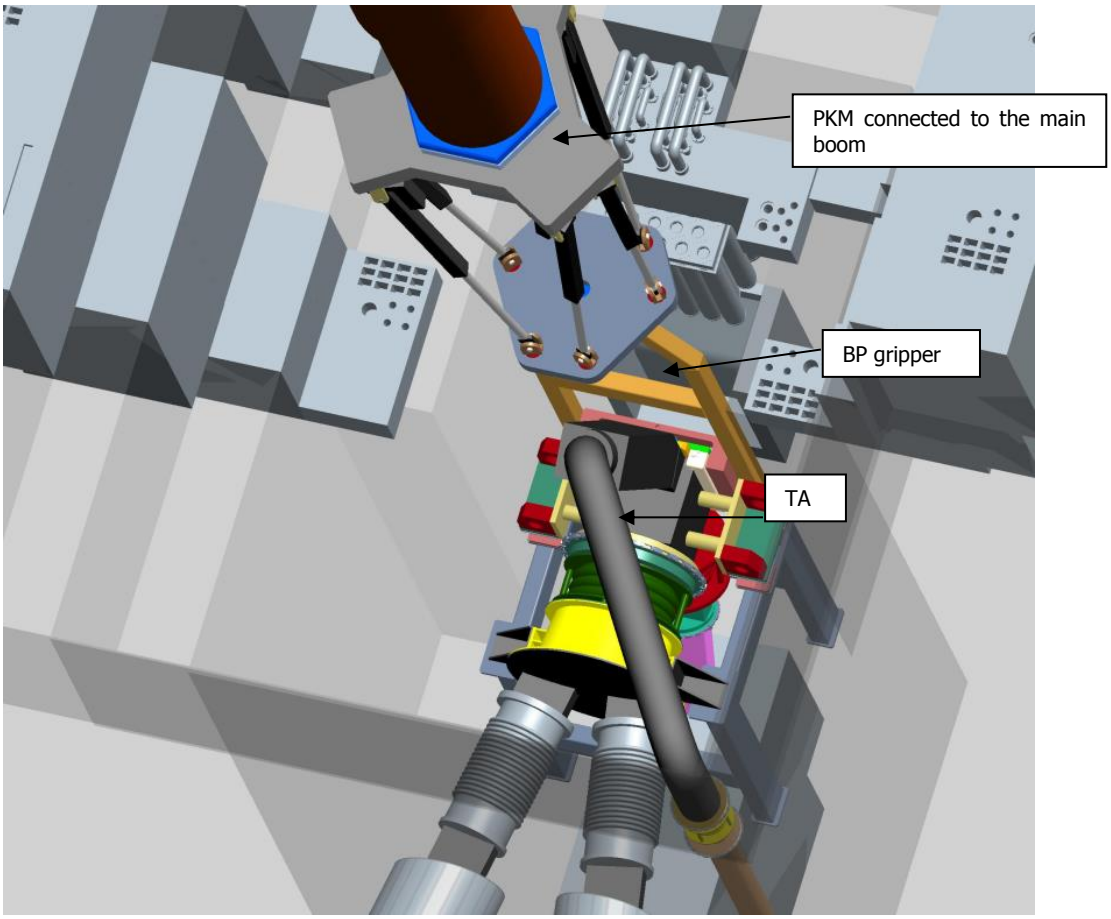

Fig. 2.21 - BP removal in Test Cell

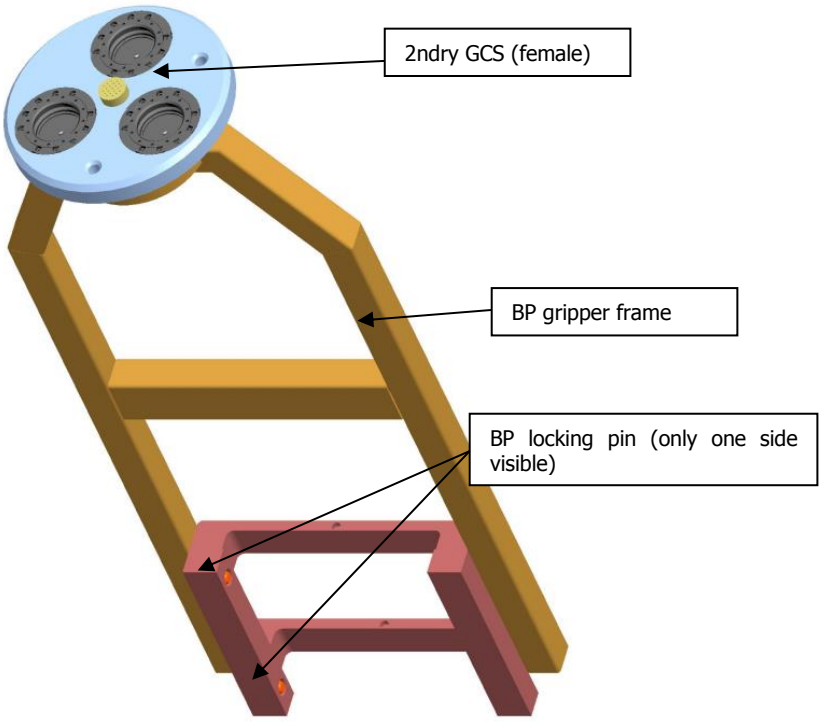

Fig. 2.22 - BP gripper overall view

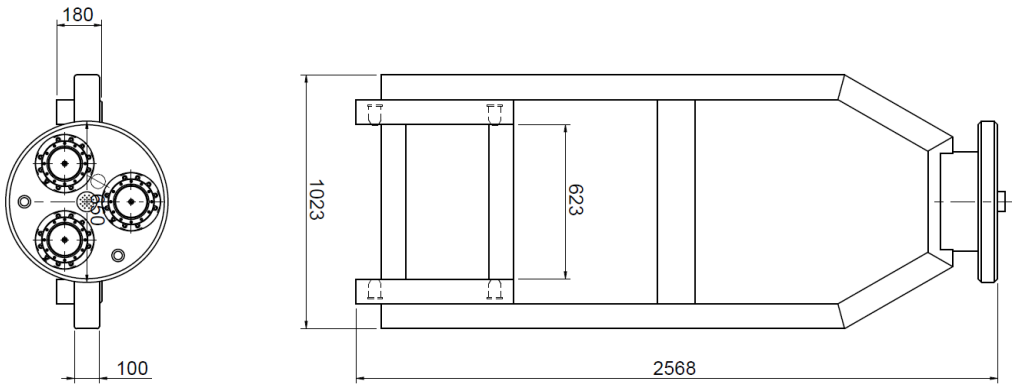

Fig. 2.23 - BP gripper dimensions

A vertical stroke of the PKM robot of 750 mm is needed to complete the extraction of the BP from TA leaving enough clearance to be then removed with the overhead crane. Sectional view on Fig. 2.24 shows the position of the BP at the end of the extraction vertical stroke.
As indicated with the dimensions on the picture:

- the BP skates are extracted from their guides for 165 mm;
- the gap from inlet nozzle and BP lower edge is 11.5 mm;
- the gap between BP gripper frame and Medium Flux Test Module (MFTM) (which, however, in "reference" condition is not in place) is 27 mm.

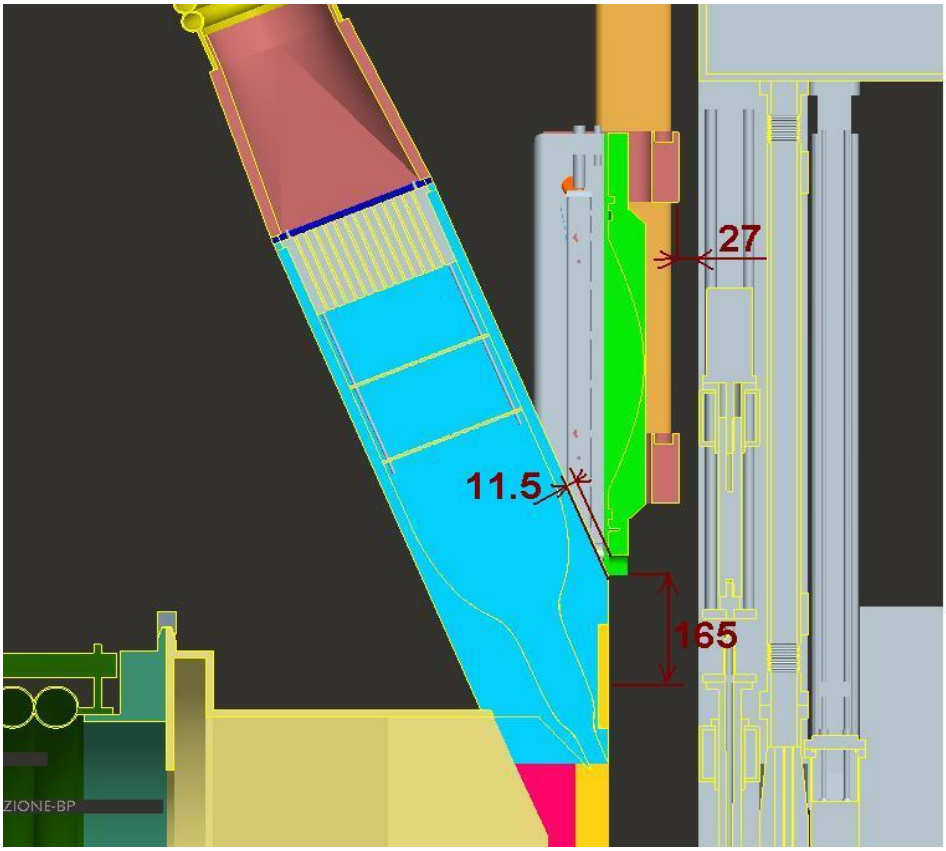

Fig. 2.24 - Gap in BP extraction

- *TA gripper*

The TA gripper is based on a machined welded frame that can be connected to the PKM tool plate. At the lower end of the frame 4 connection block link the frame with the TA. As discussed for BP gripper, TA gripper uses 4 actuated conical pins that can be positioned in three configuration:

- With pins “out” TA is free from the gripper;
- With pins “full-in” TA is rigidly connected to the gripper;
- With pins “half-in” there is some play between gripper and TA.

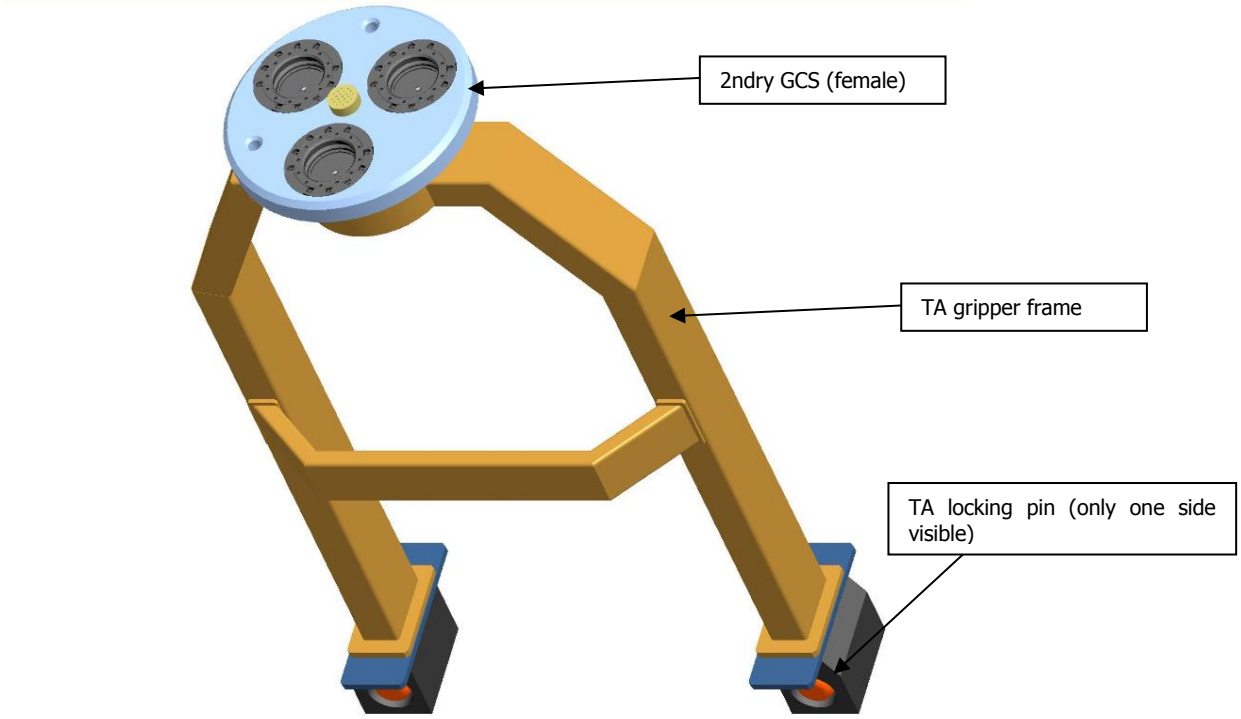

Fig. 2.25 - TA gripper overall view

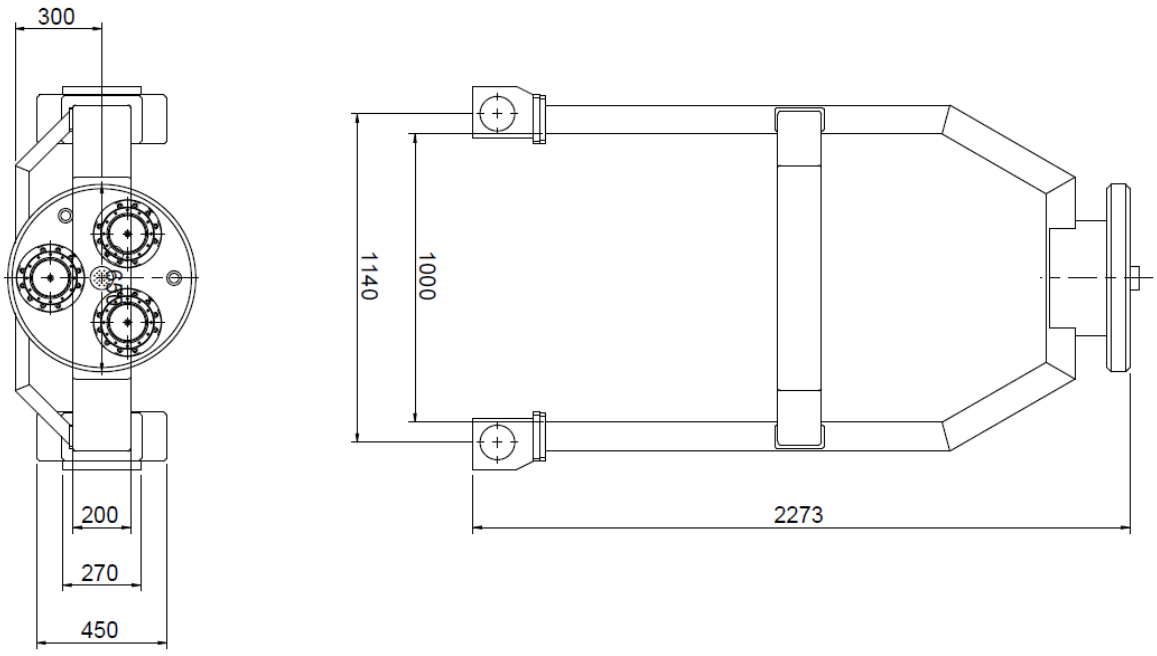

Fig. 2.26 - TA gripper dimensions

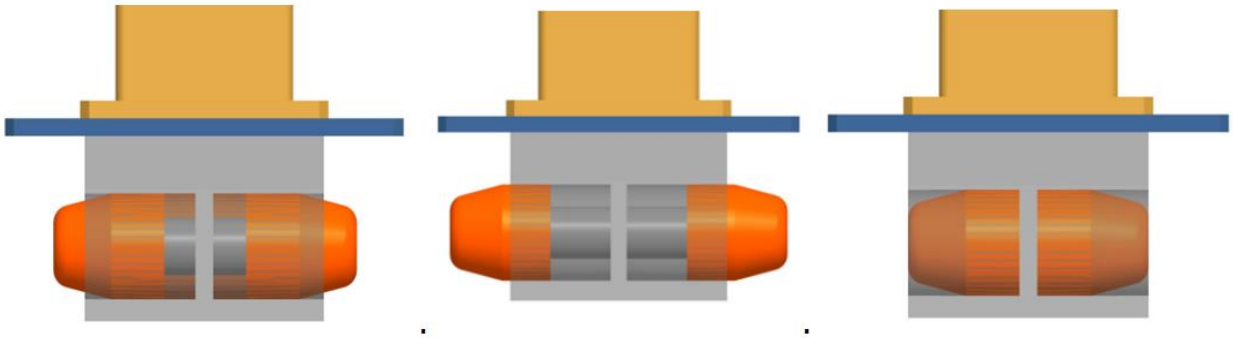

Fig. 2.27 - TA gripper three pin position

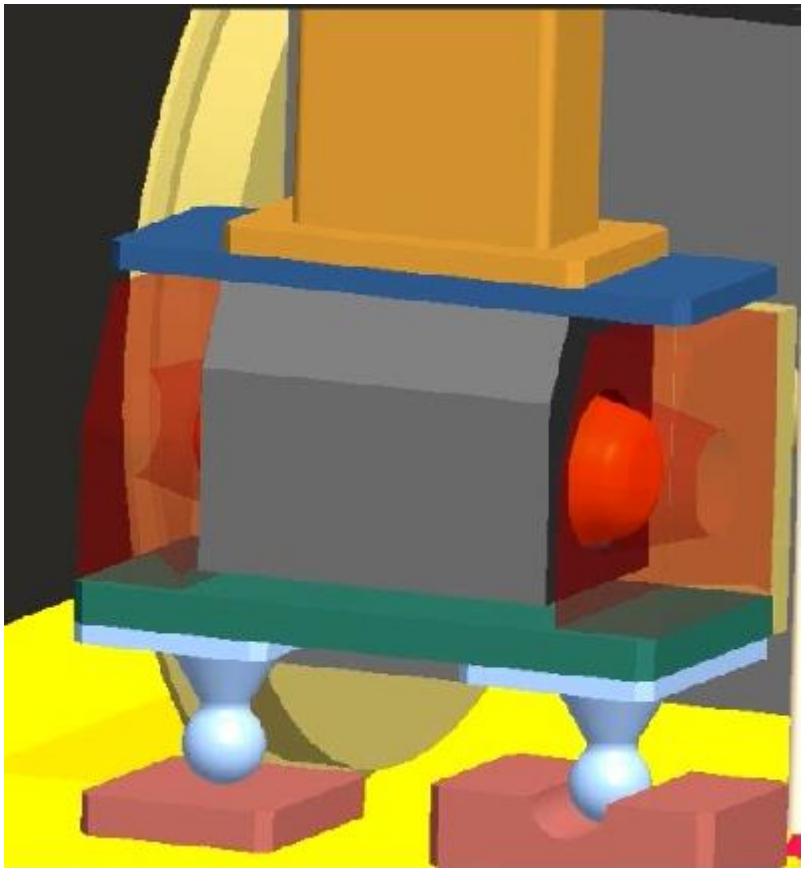

Fig. 2.28 – TA gripper in operation

- *Bolting tool*

The bolting tool can be connected at the 7 DOF robot tool plate with a quick connect/disconnect plate. The bolting head is relocated with respect to its motor with a 500 mm neck and a 90° angular head.

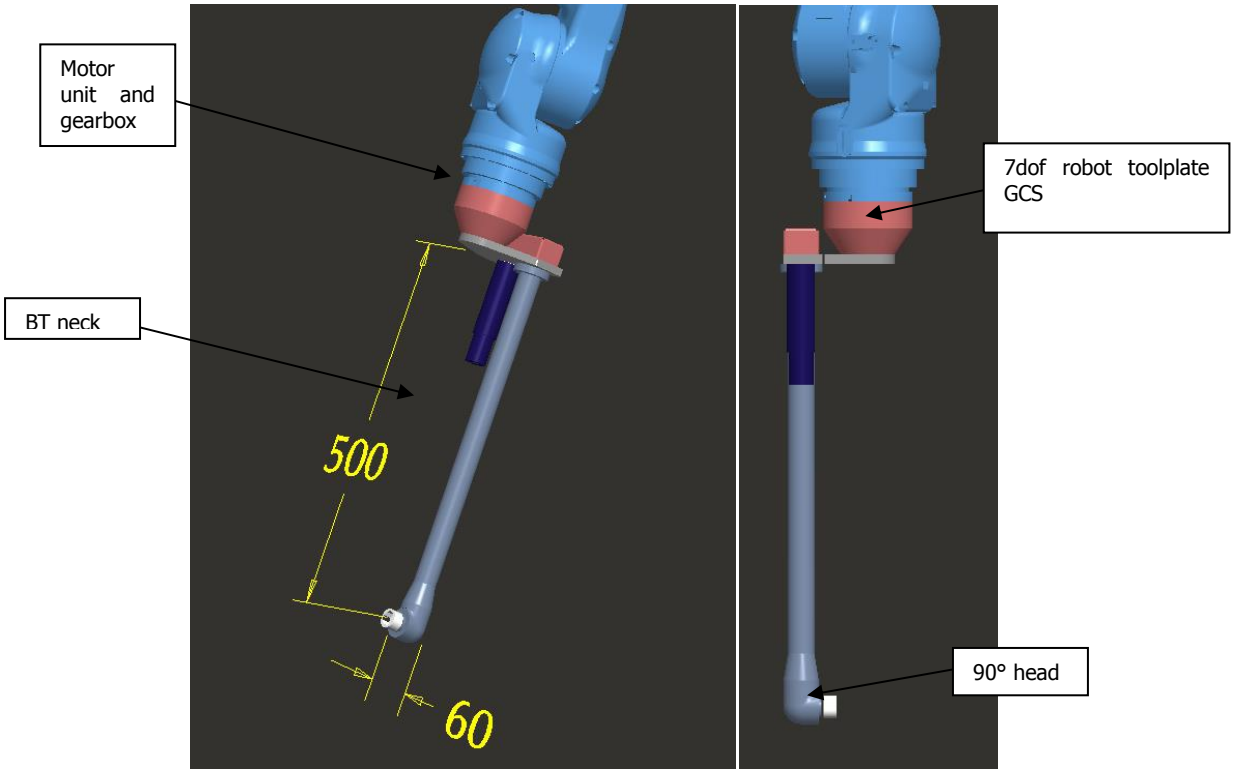

Fig. 2.29 – Bolting tool dimensions and overall configuration on robot wrist

With this configuration it is possible to access and completely extract BP docking bolts removing only HFTM that leaves 70 mm of gap between the MFTM and BP.
The following picture shows access to the BP docking screws. The bolting tool must access from above because of the shape of the internal walls of the TC that leave no lateral access to BP.

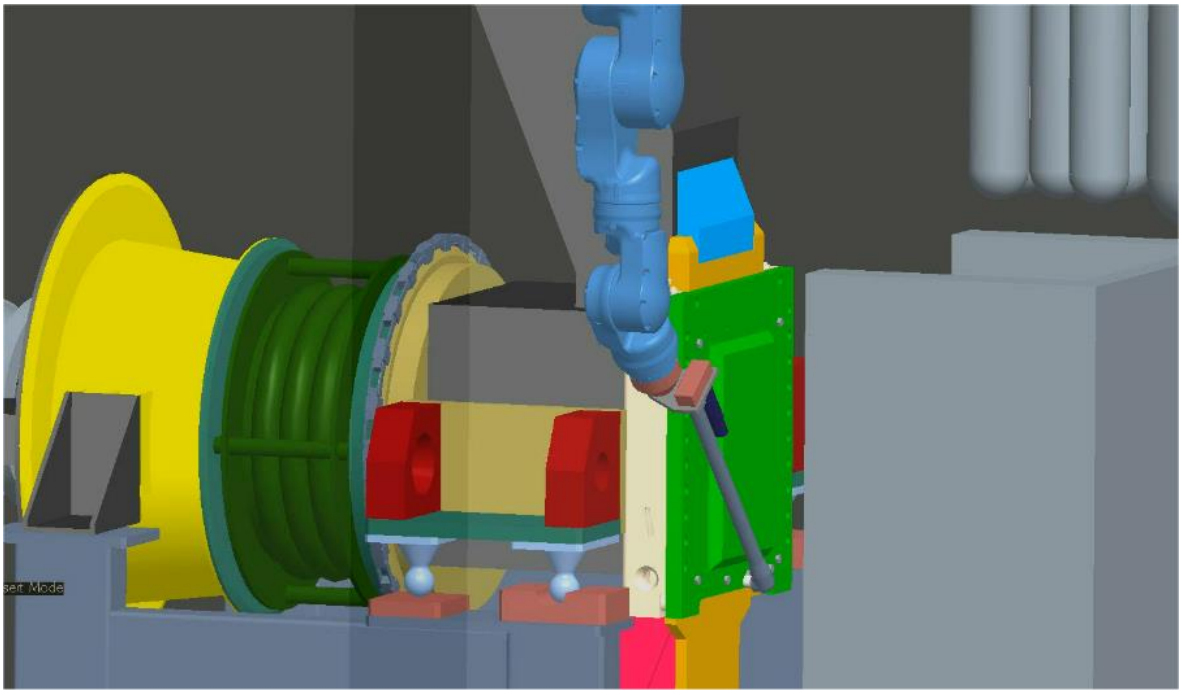

Fig. 2.30 - BP lower bolt access with HFTM and MFTM removed

- *Ribbon cleaning tool*

Ribbon clearing tool uses a continuous ribbon that is driven to “clean” to “dirt” spool with a drive motor. A dispensing head add cleaning solution to the ribbon before the cleaning head. A conceptual layout of this configuration of cleaning tool is shown in the following picture. Cleaning solution dispensing head is in blue while cleaning wheel is in red. A dedicated interface connect the cleaning tool to the robot trough a GCS that powers also the tool. The support should enable a level of compliance between the cleaning wheel and the part to be cleaned to ensure correct and uniform pressure against the surface to be cleaned. Considering the low complexity of the cleaning tool compared to the replacement of the ribbon once completely used the cleaning tool is considered in this phase as “disposable”. The bigger advantage of this configuration is that the cleaning surface is continuously kept clean (the ribbon speed is higher than cleaning head cleaning speed). The bigger limit is that, to keep ribbon in place on the cleaning wheel the cleaning direction must always stay in the cleaning wheel plane (no or low transverse displacement is possible to avoid ribbon run out of the wheels). Ribbon length, capstan speed and amount of surface clean per tool will be validated in a next dedicated mock-up and test phase.

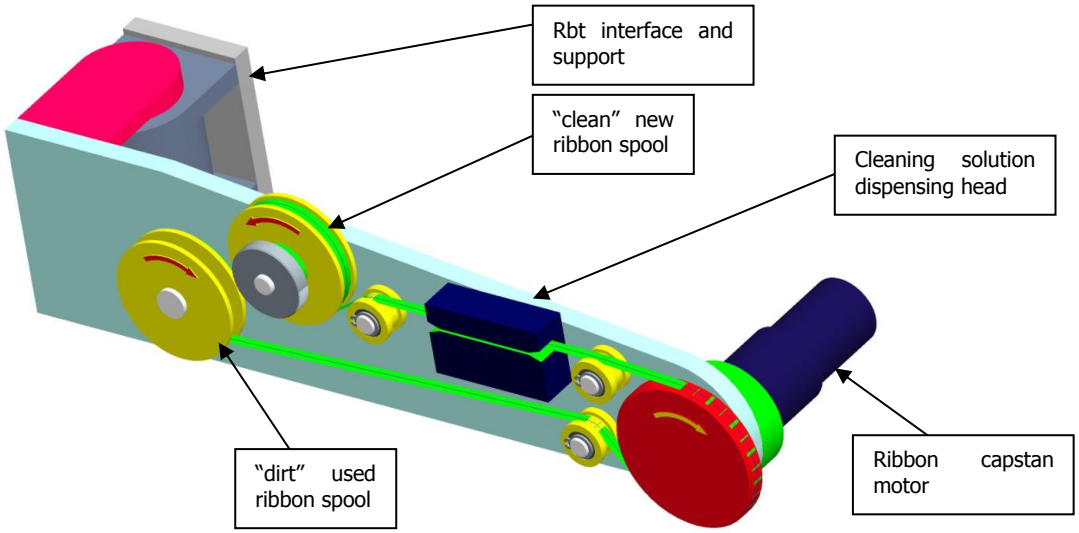

Fig. 2.31 – Ribbon CT general view

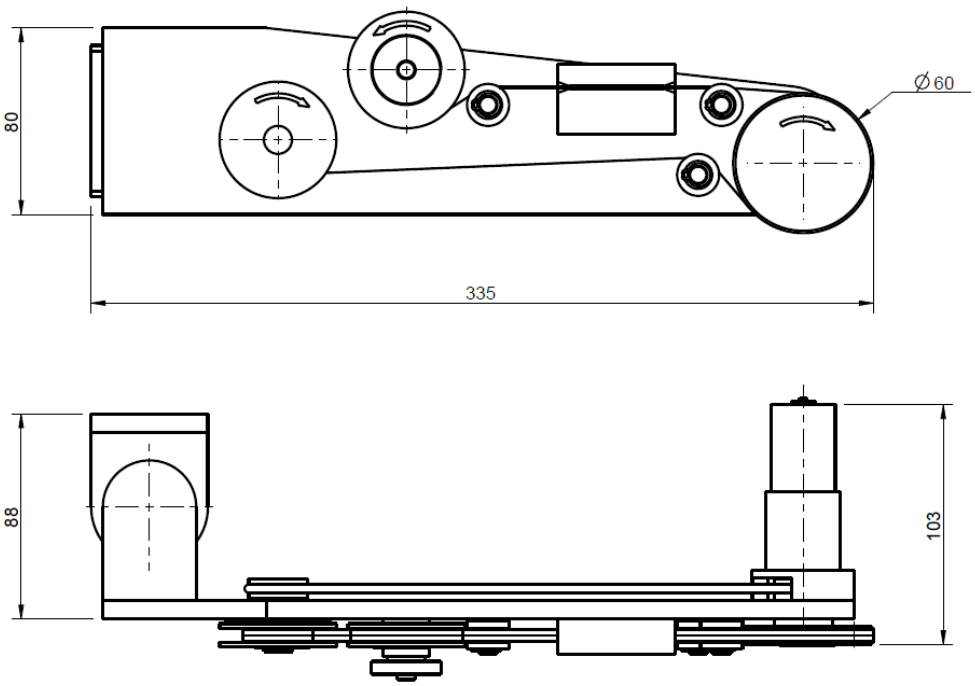

Fig. 2.32 – Ribbon CT dimensions

The following picture shows the 7 DOF robot clearing the beam FDS mating flange. The same robot+tool configuration can be used to clean inlet and outlet FDS flanges (the three tasks are performed in TA complete replacement or in TA frame cleaning for BP replacement (with HFTM and MFTM removed).

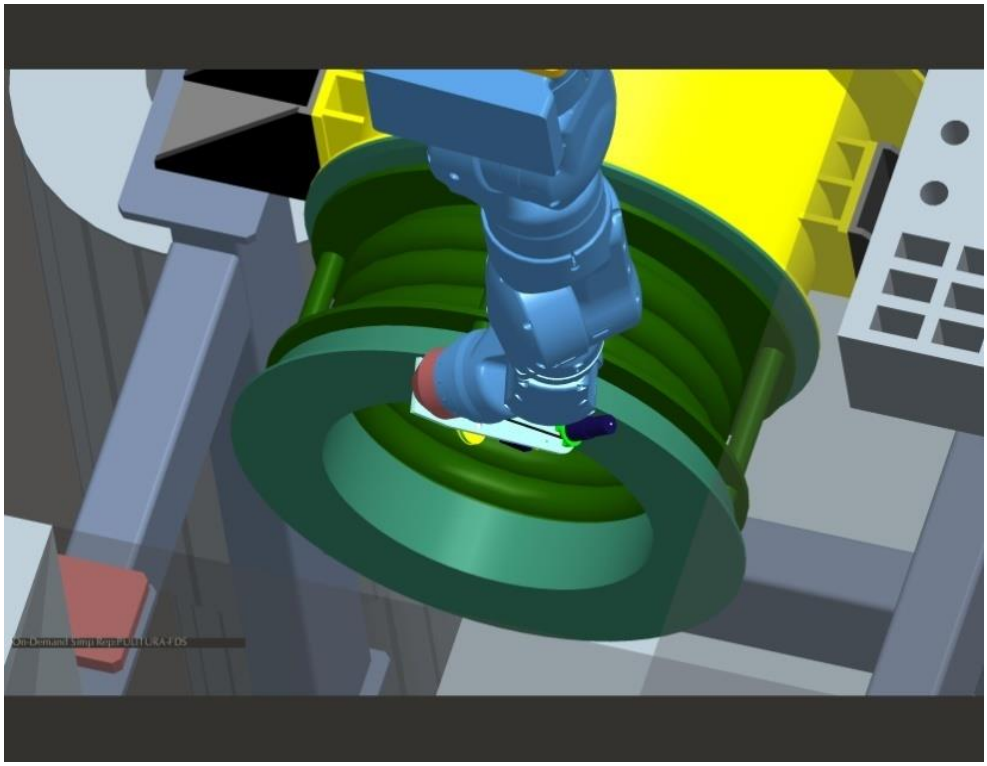

Fig. 2.33 – Ribbon CT in operation on beam FDS flange

2.2 Nuclear analysis

Neutronic calculations and nuclear responses

In order to support the engineering design activities of the system, a nuclear analysis has been carried out for the entire TA [7]. The coupled n-γ transport calculations were performed by using the MCNP-5 1.6 Monte Carlo transport code compiled in parallel version (openmpi-intel-1.2.8). The calculations were performed for 10^9 histories. The full performance operation phase consisting of two deuteron beams each of 40 MeV, 125 mA working continuously for 1 year was considered in the transport calculations (full-power year or fpy in the following).

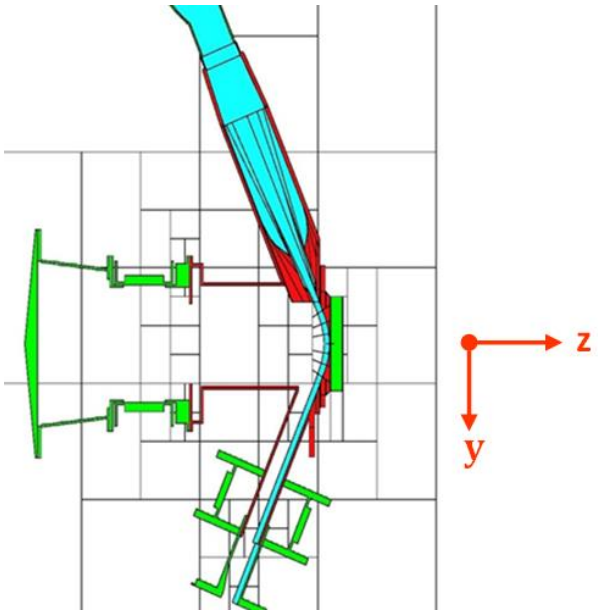

Fig.2.34 - Vertical cut at x=0 of the geometry model for the entire TA used in the MCNP calculations.

The nuclear responses calculated were mainly:

- the heat deposition due to neutrons and prompt γ's (beam-on condition),
- DPA and
- the gas production (production of hydrogen and helium due to nuclear neutron interactions with the nuclides of the structural materials).

The NRT model was applied to calculate the DPA. The DPA values were calculated for iron (Fe). The nuclear responses were obtained by multiplying each neutron spectrum by an energy dependent response function, i.e. energy dependent gas production cross sections, displacement production cross sections and heating functions. The nuclear responses values averaged on the volume of the BP corresponding to the beams footprint area (20 cm×5 cm) are shown in Table 2.

Tab. 2.4 - Nuclear responses on the BP footprint volume

Neutron Flux (n/cm^2/s)	1.36E+15
Photon Flux (n/cm^2/s)	3.92E+14
Neutron heating (W/cm^3)	1.66E+01
Photon heating (W/cm^3)	1.55E+01
Displacement Per Atom (DPA/fpy)	5.67E+01
Hydrogen production (appm/fpy)	2.97E+03
Helium production (appm/fpy)	7.28E+02

The values of heat deposition, due to neutrons and γ's, and DPA were calculated over the entire TA via the "superimposed mesh tally" feature of MCNP5 code by choosing a proper spatial mesh grid readable by the FE code. In Figures 2.35 and 2.36 the neutron and gamma heating (W/cm^3) distributions over the TA are shown.

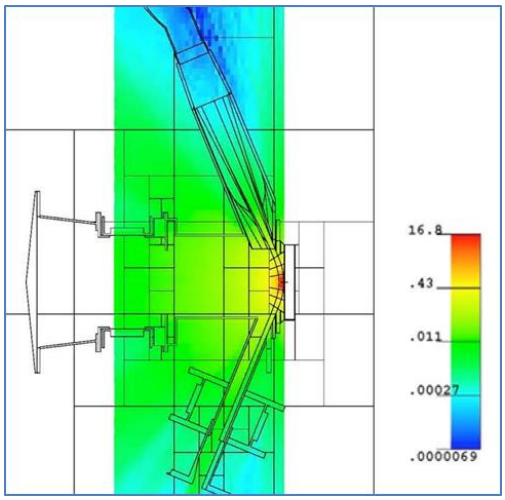

Fig.2.35 - Neutron heating (W/cm^3) distribution on TA. Vertical cut at x=0.

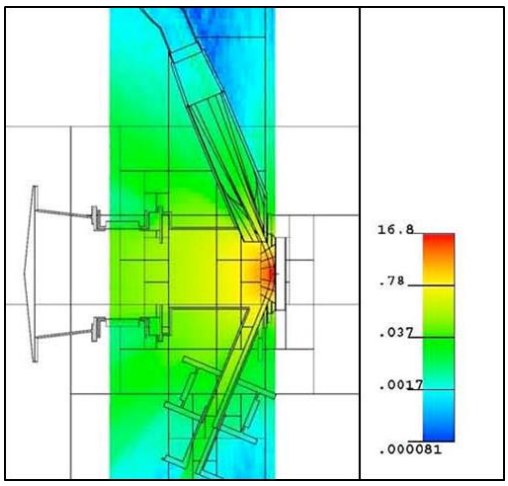

Fig.2.36 - Gamma heating (W/cm^3) distribution on TA. Vertical cut at x=0.

Neutron activation calculations

The TA+BP system is highly activated by neutron irradiation. In order to keep the neutron activation as low as possible the use of a Reduced Activation Ferritic/Martensitic (RAFM) steel (EUROFER) is foreseen as structural material for all the TA+BP components.

Neutron activation calculations were performed for the most irradiated components of the TA+BP system, namely backplate, frame, nozzle and target chamber. The aim was to provide, at selected cooling times after shutdown, radioactive inventories in terms of: a) decay heat (beam-off condition) valuable for the thermo-mechanical analysis, b) activity, contact dose rate etc., for safety purposes. These responses are

required for the overall IFMIF solid waste assessment The calculations were performed by using the EASY-2010 activation system (FISPACT code [8] + EAF 2010 neutron activation cross section data [9]).
The choice of the geometrical zones representative of each component in which to calculate the neutron spectra for the activation calculations has been a challenging job. In fact, the nozzle, for example, is about 80 cm high and the neutron flux decreases of about two orders of magnitude when moving from the zones nearest to the neutron source up to the most remote ones. The same conclusions, even if with a less strong decrease, hold for the other components as frame and target chamber. As a preliminary analysis, the neutron spectra were calculated according to the following choices: a) the averaged spectrum in the volume corresponding to the beams footprint area was considered for the backplate, b) the neutron spectra corresponding to the cells nearest to the footprint for nozzle and frame, c) the average spectrum over the cell covering the entire target chamber. The corresponding total fluxes (n/cm^2 s) are 1.36×10^{15}, 3.98×10^{13}, 2.68× 10^{13} and 9.78× 10^{12}, for the backplate, nozzle, frame and target chamber respectively. These neutron fluxes were considered as the fluxes representative of the whole component. A more refined analysis should take into account the differences of the neutron fluxes in the various parts of each component and perform the activation calculations accordingly.

The neutron spectra were calculated via the MCNP5 1.6 code with McDelicious-11 in the VITAMIN-J+ (211 energy groups structure) of the EAF-2010 group-wise neutron activation library (eaf_n_gxs_211_flt_20010). An operating scenario of 345 days (20 days a year for maintenance) was considered in the activation calculations for all the components. The calculations were performed for cooling times from shutdown up to 106 years. Several parameters are used to assess the relevance of the activation to safety and waste disposal issues, the most important of which are activity, contact γ-dose rate and decay heat.
In the Figs. 2.37-2.39 the curves of the specific activity (Bq/kg), decay heat (kW/kg) and contact γ-dose rate (Sv/h), vs. decay time, are shown for the four components.

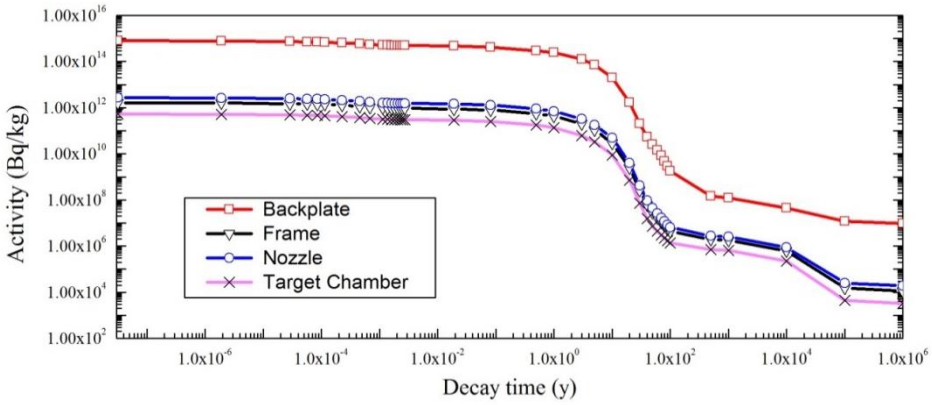

Fig. 2.37 - Activity vs. decay time

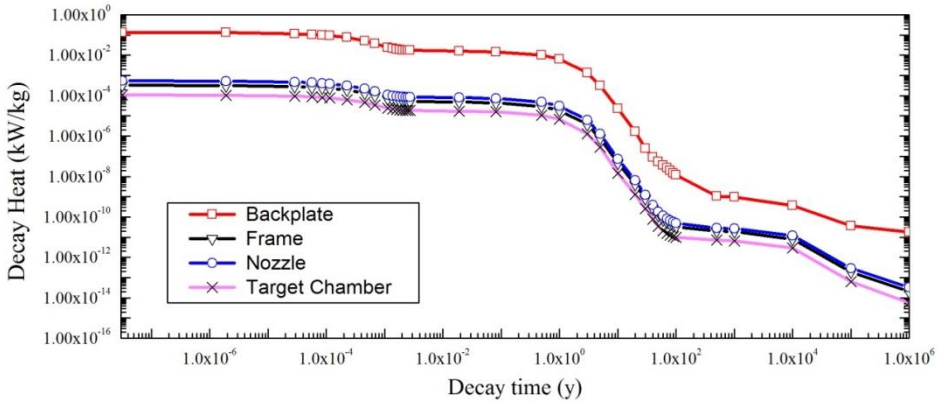

Fig. 2.38 - Decay heat vs. decay time

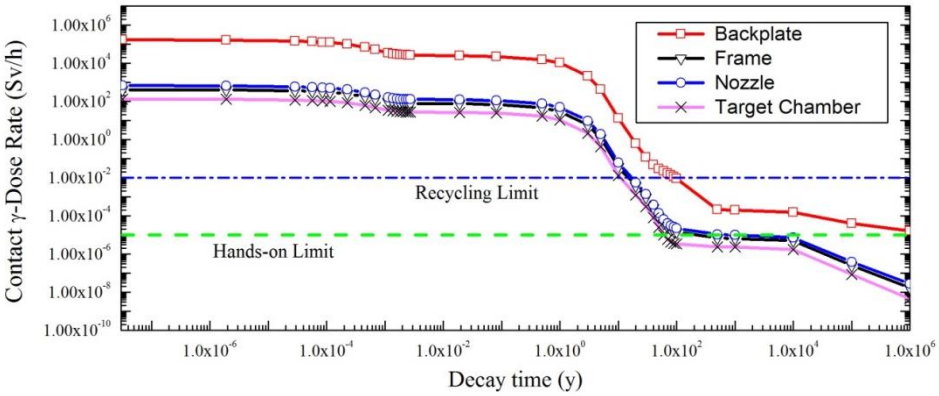

Fig. 2.39 - Contact γ-dose rate vs. decay time

2.3 Thermomechanical analysis

With the objective of evaluating the performances of the system and supporting the engineering design activities, an uncoupled thermomechanical analysis has been performed in close collaboration with the University of Palermo by means of a qualified finite element (FE) thermomechanical code. The calculations employed a realistic 3D FE model which takes into account all mechanical and thermal loads including the nuclear heating due to neutron and gamma fields generated in the liquid target, which has been calculated as part of the neutronic analysis (see Sect. 2.2).

The finite element discretization employed in the thermomechanical model is shown in Fig. 2.40. A mesh independency analysis has been performed to select an optimized mesh which allows accurate results to be obtained saving calculation time. A mesh composed of ~207000 nodes connected in ~880000 tetrahedral elements has been selected, which allows numerical simulations to be carried out in about 9 hours.

Reduced activation ferritic/martensitic (RAFM) steel EUROFER has been considered as TA structural material. Lithium flow has been modeled too in order to properly simulate its thermal interaction with the TA. Materials have been considered homogeneous, uniform and isotropic. A linear elastic mechanical behavior has been assumed for the EUROFER.

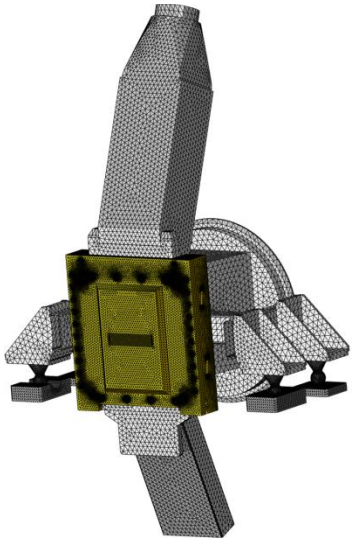

Fig. 2.40 - FE computational mesh

Loads and boundary conditions

The following thermal loads and boundary conditions have been adopted:

- Volumetric density of nuclear heat power deposited in the footprint region of the lithium flow. An average value of 40 GW/m^3 has been assumed.
- Volumetric density of nuclear heat power deposited within the TA, as calculated by a nuclear analysis performed through the MCNP transport code (Fig. 2.41)
- Forced convection between lithium and TA surfaces assuming a constant convection heat transfer coefficient of 34000 W/m^2 K [10-12]
- Heat transfer between BP and High Flux Test Module (HFTM) by radiation and conduction through the He gap assuming He in the Test Cell (TC) at nominal conditions. HFTM surface has been assumed at 50 °C.
- Conduction heat transfer between target chamber and beam duct. This has been modeled through a convective-type heat transfer coefficient assumed equal to 15.8 W/m^{2}K according to [6], and a non uniform bulk temperature analytically derived from a 1D simplified model of the conductive-radiative heat transfer in the beam duct
- Internal irradiation between lithium free surface and TA internal surfaces (Fig. 2.42). EUROFER and Li emissivities have been assumed equal to 0.3 and 0.06, respectively [10-12]
- External irradiation between target chamber and TC environment and between external surface of BP and frame and that of HFTM (Fig. 2.43)

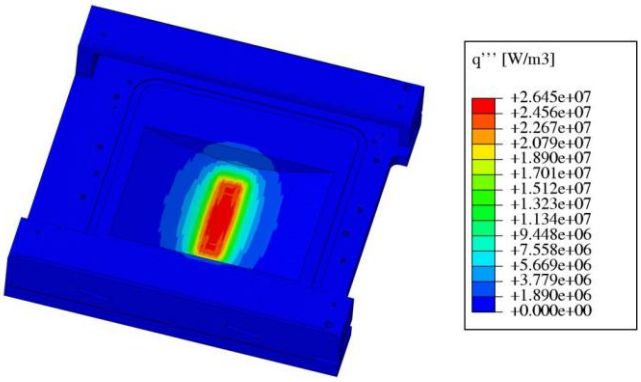

Fig. 2.41 - Nuclear heat power deposition in the BP

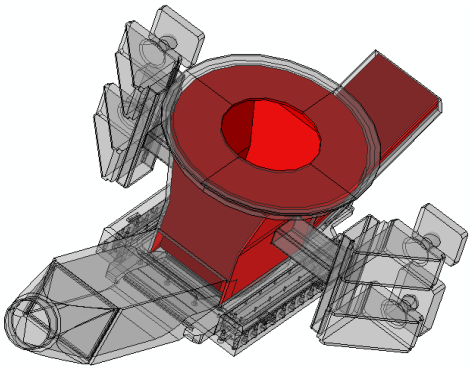

Fig. 2.42 - Internal irradiation surfaces (in red)

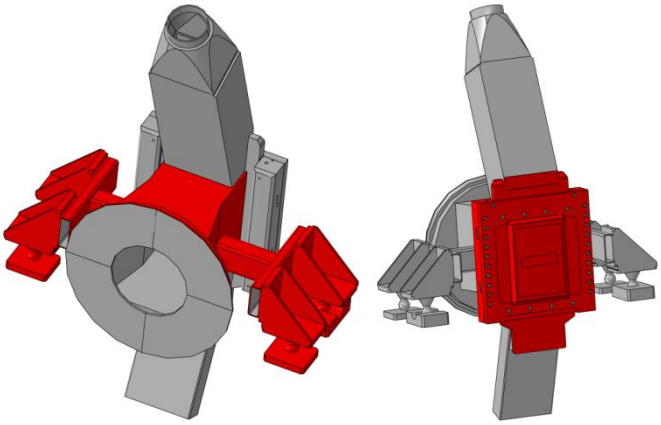

Fig. 2.43. - External irradiation surfaces (in red)

The following mechanical loads and boundary conditions have been included:

- Thermal deformations
- Internal and external pressures on the TA. Internal pressure has been applied to lithium wetted surfaces according to the results of the thermohydraulic analysis
- BP tightening screw loads
- Skate-based clamping system loads
- TA constraints

Operating conditions

The analysis has been performed considering the steady state nominal conditions which are specified as follows:

- Li temperature at nozzle inlet: 250 °C
- Li velocity at nozzle inlet: 15 m/s
- TA internal pressure: 10^{-3} Pa
- TA external conditions: He gas, p=10 kPa ; T=50 °C
- HFTM external surface temperature: 50 °C

The results of the thermomechanical analysis are reported hereafter in terms of temperature, stress and displacement fields in the whole TA and in the BP alone.

Calculation results

Fig. 2.44 shows the temperature distribution in the whole TA while the detail of the temperature field in the BP is reported in Fig. 2.45. It can be seen that a maximum temperature of about 400 °C and 475 °C is respectively achieved in the two components, which meets the favorable EUROFER operational temperature range (350-550 °C roughly).

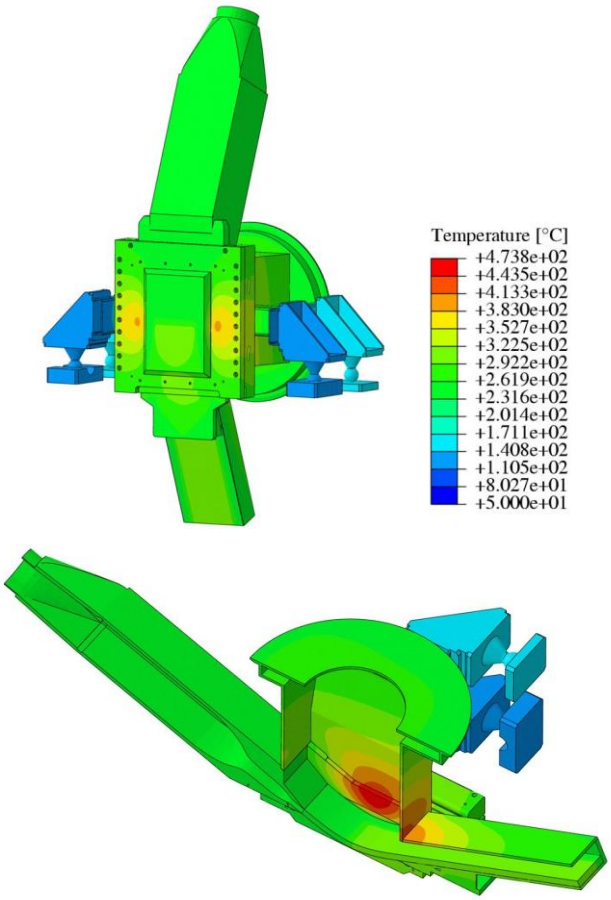

Fig. 2.44 - Temperature distribution in the TA

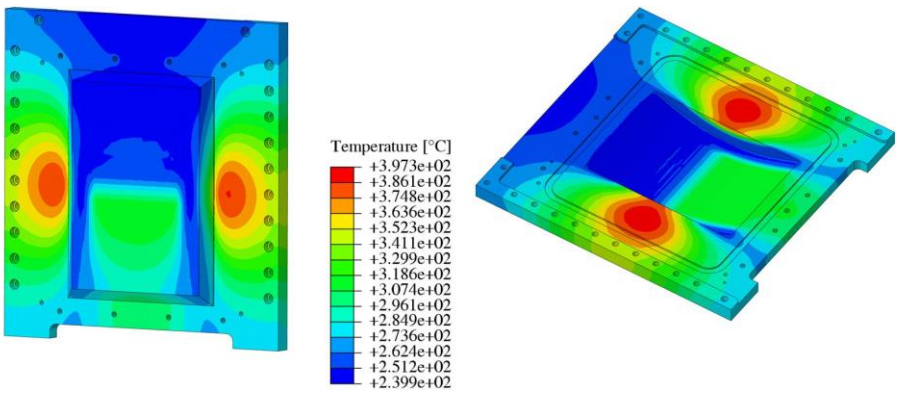

Fig. 2.45 - Temperature distribution in the BP

The Von Mises equivalent stress field arising due to the total (mechanical+thermal) load applied is reported in Fig. 2.46 and Fig. 2.47 for the whole TA and the BP, respectively. Results indicate that the yield strength of the material is not reached anywhere in the system except that in very small, localized regions on the BP, thus not posing any critical issues from the structural integrity point of view. This can be better seen by plotting the Ω-parameter defined as the ratio of the Von Mises stress to the material yield strength (as a function of the temperature field), which is shown in Fig. 2.48.

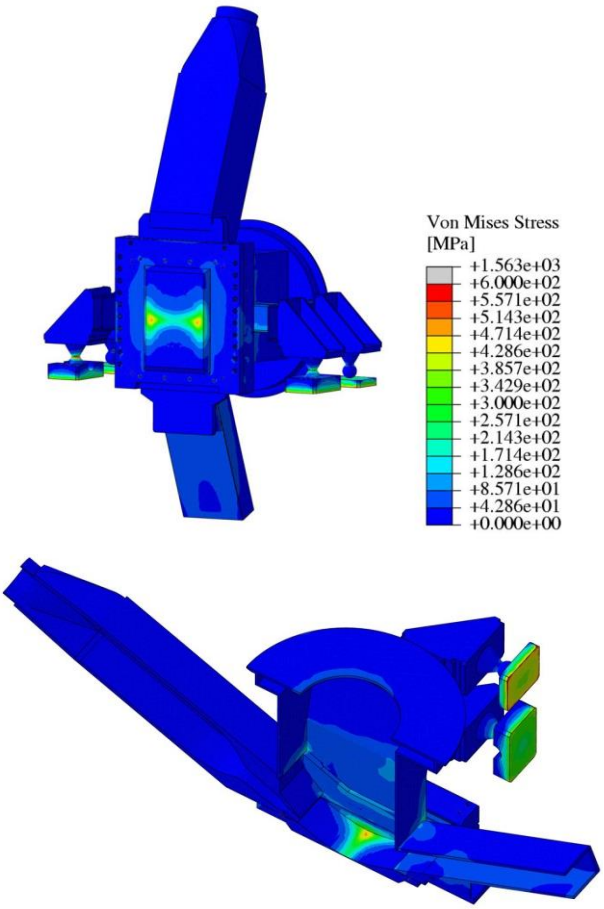

Fig. 2.46 - Von Mises equivalent stress field in the TA

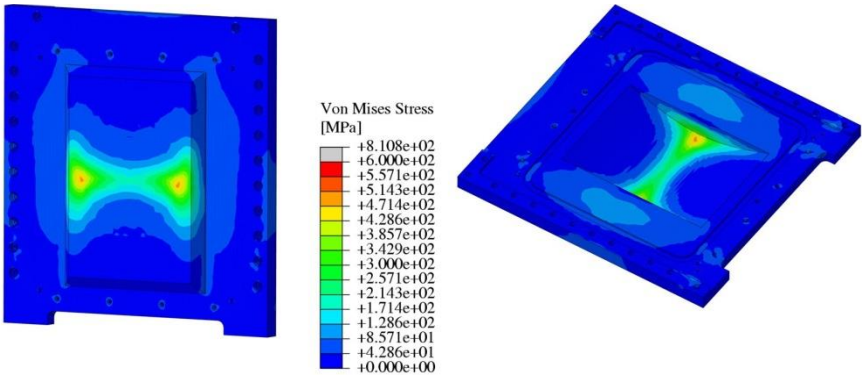

Fig. 2.47 - Von Mises equivalent stress field in the BP

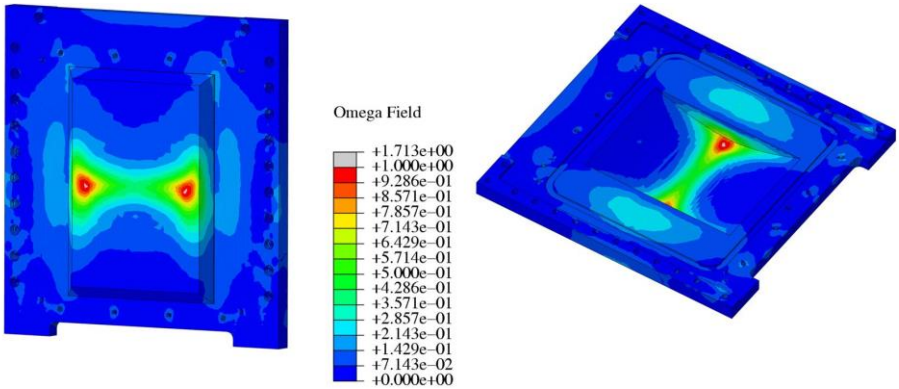

Fig. 2.48 - Ω-parameter field in the BP

Fig. 2.49 reports the BP displacement field along the beam direction (U_y). A maximum displacement of 2.513×10^{-4} m is found at the point nearest to the HFTM. Therefore, no contact is foreseen between BP and HFTM. Moreover, the IFMIF design requirement that stipulates a BP-HFTM gap dimension of 2±1 mm [4,6] is fulfilled under nominal scenario.

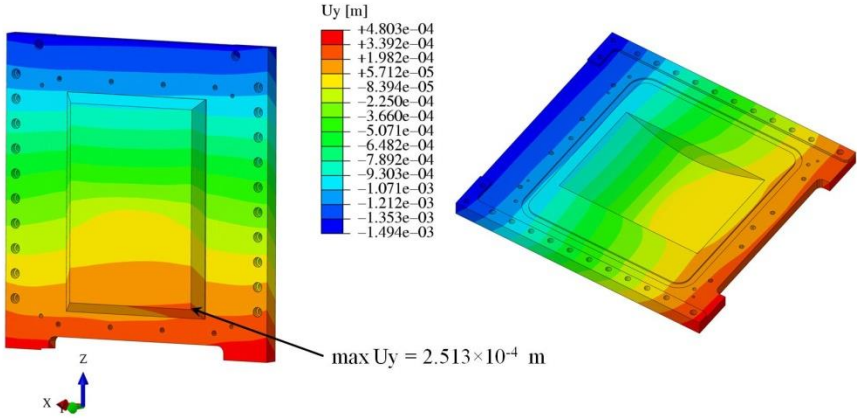

Fig. 2.49 - Displacement field along beam direction in the BP

2.4 Thermohydraulic analysis

Thermohydraulic calculations of the TA have been performed by the University of Bruxelles (ULB) through the FLUENT code. The speed of the liquid Lithium flow through the nozzle and the open channel is low enough for the flow to be considered incompressible. However, the bulk Reynolds number Re reaches a value of $38\text{x}10^3$ (in the nominal case) so that it is fully turbulent. The flow is further characterized by the Weber number which measures the relative importance of inertial effects and surface tension effects. In all cases considered in this study, We>>1 so that surface tension effects can be neglected (in the nominal case, $We\approx10^{13}$).

To model turbulence, the k-ε model has been used. Earlier computations [13] on IPPE geometry flows [14] showed that all turbulence models available in FLUENT predicted similar bulk parameters and near wall characteristics. Hence for the current study, only the k-ε was considered since it is the most efficient in terms of computational time. This model was used with the default parameters available in FLUENT. The multiphase nature of the flow in the open channel was modeled by the VOF (volume of fluid) method

coupled with Level Set method. Walls were treated as no-slip adiabatic boundaries. For the outlet boundaries, a pressure-specified condition, equal to that assumed in the TA chamber (10^{-3} Pa), was applied. The heating from the deuteron beams was simulated by using a source term in the energy equation computed through the heat deposition profile previously provided by the neutronic calculations. The computational domain is shown in Fig. 2.50.

The results of the calculations are presented hereafter for the case of steady flow at nominal conditions. In all the figures, the results at different downstream positions are reported at 7 locations and labeled from A to G (see Fig. 2.50)

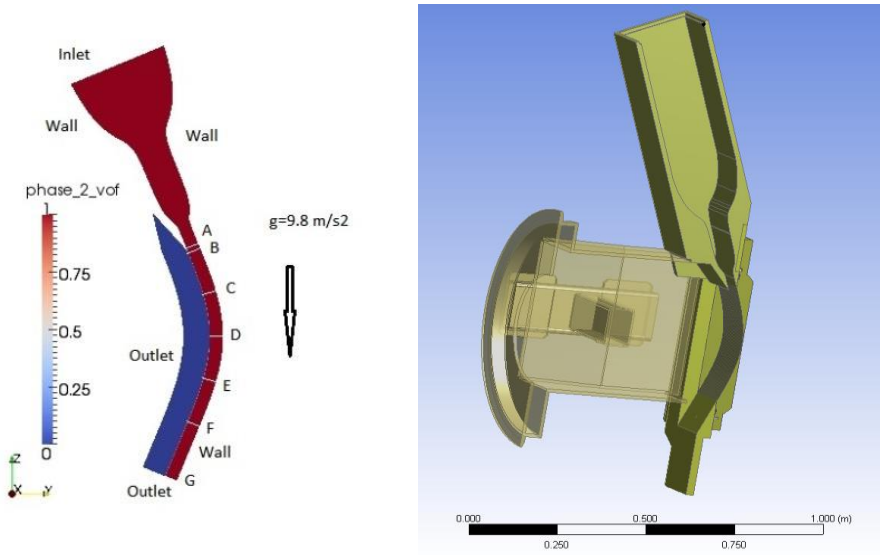

Fig. 2.50 – Computational domain for thermohydraulic analysis. The figure on the left shows the volume fraction of Li

Fig. 2.51 show the plots of streamwise velocity as a function of distance from the wall at the various locations marked in 2.50 on the center plane of the domain. The velocity profile progressively relaxes from its shape in the bounded domain corresponding to the nozzle, to a free surface flow shape as the liquid moves downstream. The boundary layer at the wall on the nozzle exit (green line) is very thin and grows downstream of the domain. The steepness of the velocity profiles on the back-plate decreases till the center of the curved section (due to curvature effects) and increases again as the flow reaches the straight section and finally the exit. As is clear from these profiles, the jet initially thickens after exiting the nozzle from 25 mm to about 26.5mm at the center of the curvature; the thickness then decreases back to about 25 mm towards the exit.

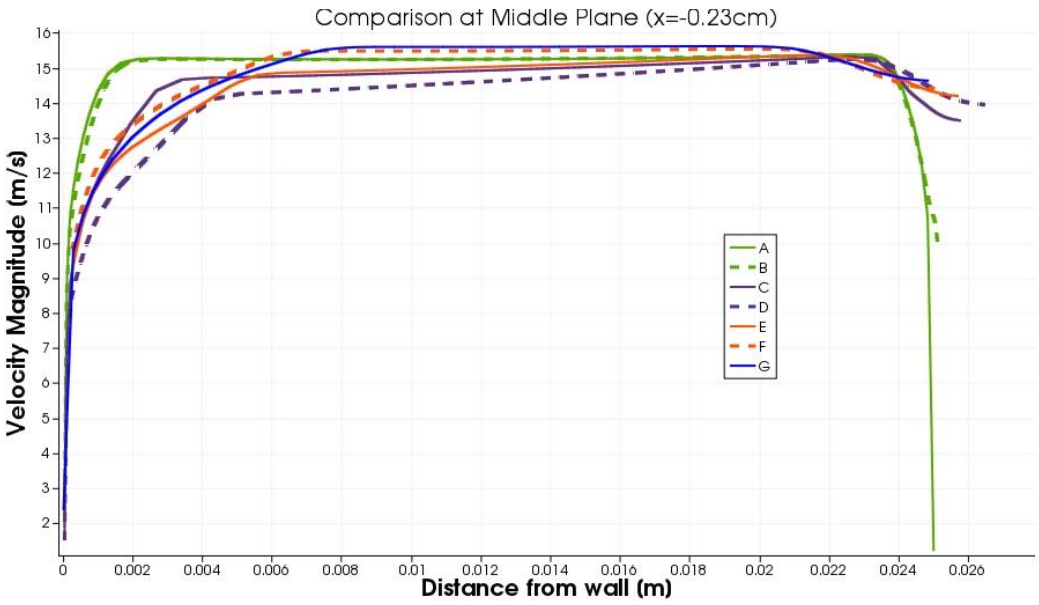

Fig. 2.51 - Streamwise velocity profiles as a function of the distance from the wall across the Li flow at locations A to G and at the middle plane of the domain.

Pressure profiles at the same locations (the reference pressure is set at 10^{-3} Pa at the exit of the domain) are shown in Fig. 2.52. We note that the pressure increases as the flow goes over the curved section due to centrifugal forces and reaches its maximum value of about 12 kPa at the center of the curved section on the backplate. The pressure at the interface is very similar for all the locations although not identical.

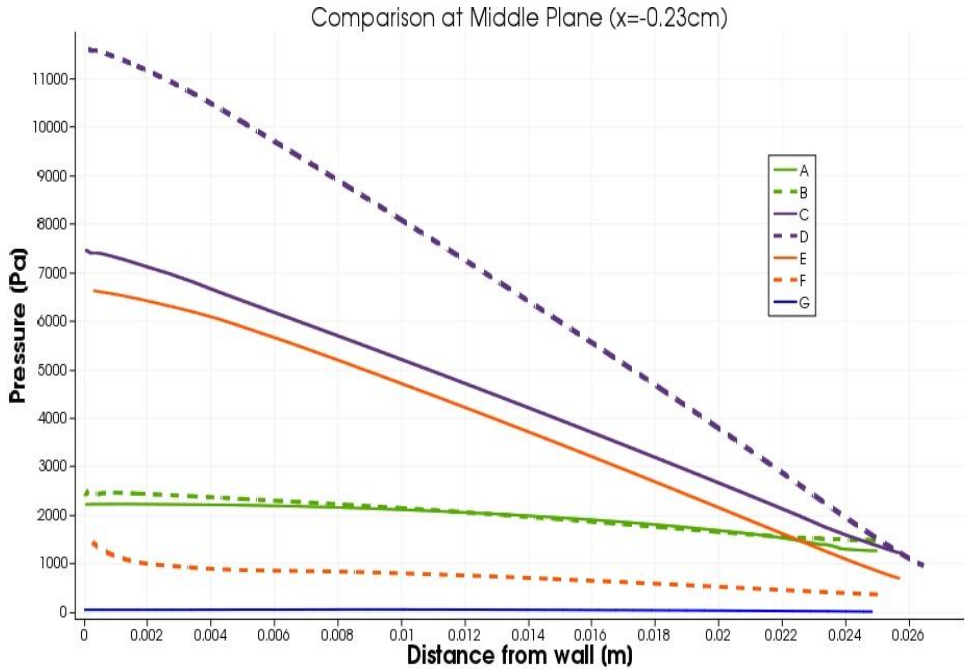

Fig. 2.52 - Pressure variations across the Li flow at locations A to G and at the middle plane of the domain. Reference pressure is set at 10^{-3} at the outlet G.

Fig. 2.53 shows the pressure variation along the back wall at the middle section of the computational domain. The pressure is highest at the inlet of the nozzle and decreases as the velocity increases till the nozzle exit where the Li jet emerges with a velocity of 15 m/s. Pressure then gradually increases on the curved back plate (due to the curvature) till the center, after which it again decreases till the straight section. The slight slope along the straight section is due to viscous losses. Artifacts in the pressure at locations B,F are related to changes in mesh topology at these locations. Contours for pressure along the middle section are shown in Fig. 2.54 and clearly highlight the role of curvature in the pressure field distribution.

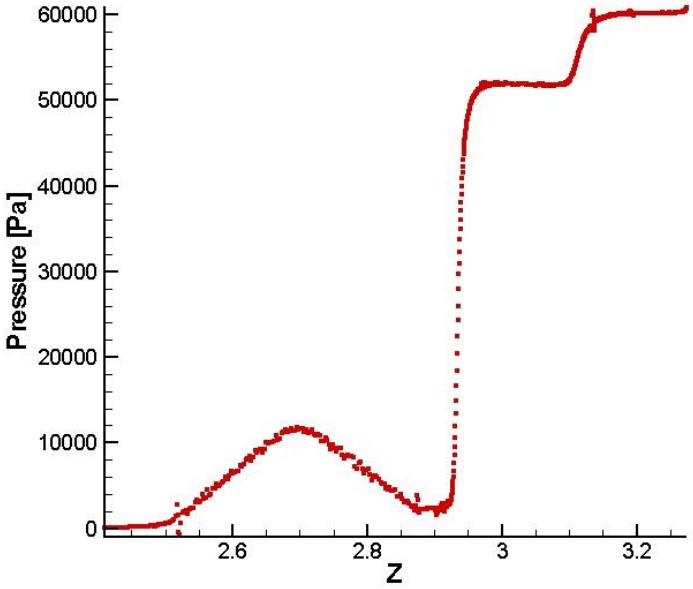

Fig. 2.53 - Pressure along the back-wall at the middle section.

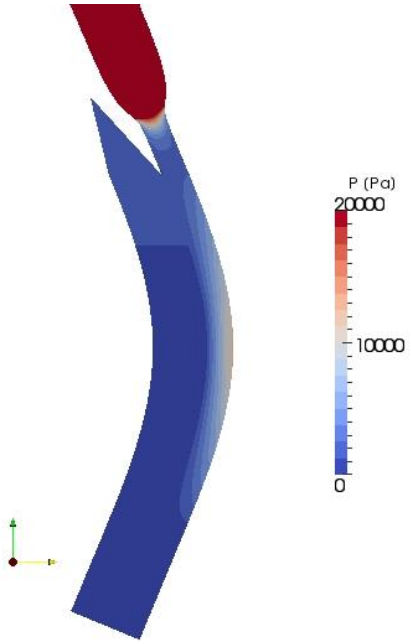

Fig. 2.54 - Pressure contours at the middle section

Fig. 2.55 shows the contours of temperature on the surface of the Li jet (defined as volume fraction of 0.5 for Li) on the left and on the middle plane on the right. Also marked are the locations A to G by black points with labels next to them. Variation for temperature contours mimics the heating pattern closely. This is because of the high velocity of the flow and the fact that convective energy transport dominates (there is little diffusion of heat as discussed later). As is noticeable on the surface contours, the peak heating occurs at side locations away from the central plane (the two red streaks at the edge) and at the center of the spanwise direction (the middle red streak line). The peak heating occurs close to the wall while keeping a safe distance from it as can be seen from the blue band of low temperature fluid between the red high temperature band and the wall. This is quantitatively shown in Fig. 2.56 where the temperature profiles are plotted as a function of the distance from the wall at different downstream locations. Note that the peak temperatures occur somewhere between the center of the back-plate and the end of the curved section (location E is midway between the center of the back-plate and the end of the curved section). Also noticeable is the fact that the temperature falls sharply almost to the inlet value at the walls. Even with adiabatic walls the temperature rise at the walls is negligible for locations A to F. Only at location G there is a slight increase in temperature noticeable. The temperature curves flatten from E to G due to turbulent diffusion.

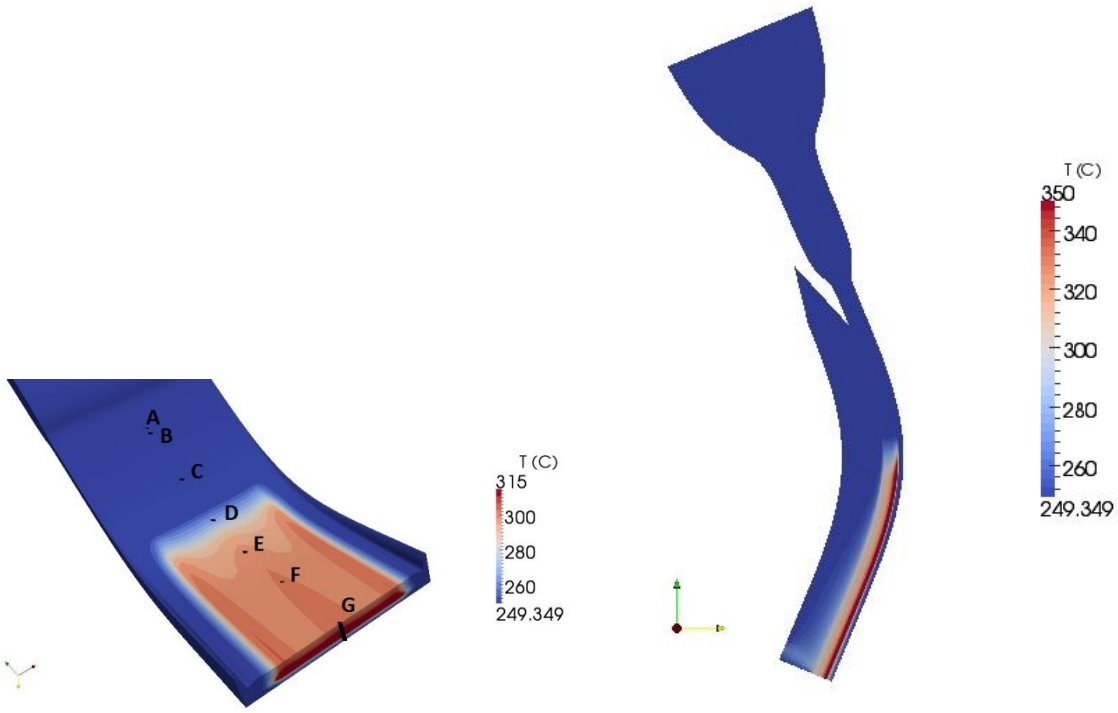

Fig. 2.55 - Temperature contours on the surface (left) and on the middle plane (right).

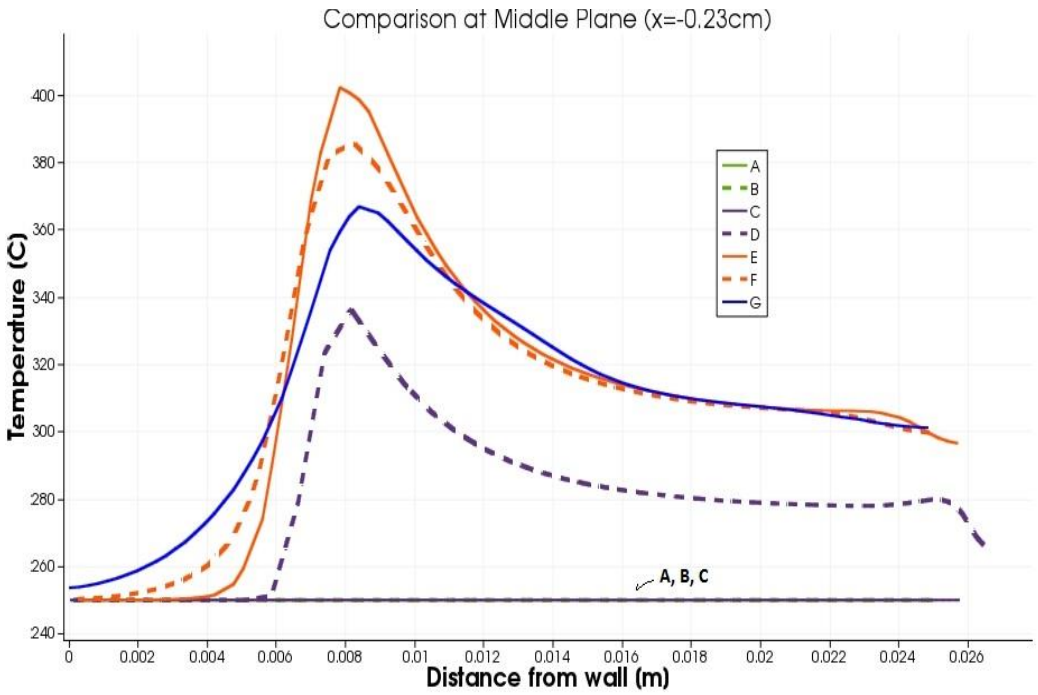

Fig. 2.56 - Temperature vs distance from wall at locations A to G on the middle plane.

3 Conclusions

In the reference period covered by the present MSE-ENEA Agreement, the design of the IFMIF TA with bayonet backplate has been advanced to a well-consolidated stage, although some work still remains to be done to fully achieve a complete and optimized configuration.

Extensive numerical analyses have been performed to support the design activities. In particular, nuclear, thermomechanic and thermohydraulic simulations have been carried out, all showing a general good matching between the TA performances and the design specifications.

4 References

1. D. Bernardi, Procurement Arrangement PA ED03-EU, IFMIF DMS BA_D_2233KM
2. M. Ida, Procurement Arrangement PA ED03-JA, IFMIF DMS BA_D_224QLM
3. D. Bernardi et al., “Rapporto preliminare del progetto del target di IFMIF comprensivo di disegni, analisi numeriche e valutazione dei costi”, MSE-ENEA Agreement Report, RdS/2012/265, 2012
4. D. Bernardi, “Design Description Document (DDD-III) - Target assembly with bayonet backplate”, IFMIF DMS BA_D_22W67Z, 2013
5. P.A. Di Maio, R. Giammusso, G. Miccichè, “On thermo-mechanical issues induced by irradiation swelling inside the back-plate of the IFMIF target assembly”, Fusion Engineering and Design, Vol. 86, No.6-8, p. 2597 (2011)
6. M. Ida, DDD-III_ED03JA, IFMIF DMS BA_D_22CXHK
7. M. Frisoni, D. Bernardi, G. Miccichè, M. Serra, “Nuclear Analysis of the IFMIF European Lithium Target Assembly System”, Proc. ISFNT-11, Barcellona, 2013
8. R. A. Forrest, FISPACT 2007 User Manual, UKAEA FUS 534, 2007
9. J.Ch. Sublet, L. W. Packer, J. Kopecky, R. A. Forrest, A. J. Koning and, D. A. Rochman, “The European Activation File: EAF-2010 neutron-induced cross section library”, CCFE-R (10)05
10. P. Arena, D. Bernardi, G. Bongiovì, P.A. Di Maio, G. Miccichè, “On the thermomechanical behavior of the European target assembly design of IFMIF-EVEDA lithium test loop under start-up transient scenarios”, Fus. Eng. Des., http://dx.doi.org/10.1016/j.fusengdes.2013.02.130, in press
11. P. Arena et. al., “Engineering design and steady state thermomechanical analysis of the IFMIF European lithium target system”, Proc. of SOFE-25 Conference, San Francisco (USA), 2013, in press.
12. P. Arena et al., “Analysis of the thermomechanical behaviour of the IFMIF bayonet Target Assembly under design loading scenarios”, submitted to IEEE Transactions on Plasma Science (2013).
13. A. Prakash, S. Kakarantzas, D. Bernardi, G. Micciche, V. Massaut and B. Knaepen, “Numerical simulations of the EVEDA and IFMIF lithium,” in 27th Symposium on Fusion Technology (SOFT 2012), Liege, 2012
14. N. Loginov, “The thermal-hydraulic and technological investigations for validation of the project of lithium circulation loop and neutron lithium target for IFMIF,” Obninsk, 2006.

5 Acronyms

BP	Backplate
TA	Target Assembly
BT	Bolting Tool
CT	Cleaning Tool
DDD	Design Description Document
DOF	Degrees of Freedom
dpa	displacement per atom
EDA	Engineering Design Activities
ELTL	EVEDA Lithium Test Loop
EVEDA	Engineering Validation and Engineering Design Activities
FDS	Fast Disconnecting System
GCS	Gripper Change System
HFTM	High Flux Test Module
IFMIF	International Fusion Materials Irradiation Facility
IPPE	Institute for Physics and Power Engineering
JAEA	Japan Atomic Energy Agency
MFTM	Medium Flux Test Module
PA	Procurement Arrangement
PKM	Parallel Kinematic Manipulator
RAFM	Reduced-Activation Ferritic /Martensitic
RBT	Robot
RH	Remote Handling
TC	Test Cell